TÉCNICO LISBOA

Vascularization of hepatic structures in a microfluidic platform

Diogo Miguel de Vasconcelos Resende Marques

Thesis to obtain the Master of Science Degree in

Biomedical Engineering

Supervisor: Prof. Pedro Miguel Baptista
Prof. Cláudia Alexandra Martins Lobato da Silva

Examination Committee

Chairperson: Prof. Maria Margarida Fonseca Rodrigues Diogo
Supervisor: Prof. Pedro Miguel Baptista
Members of the Committee: Prof. Cristina Maria Santos Alves de Carvalho Barrias

November of 2021

Acknowledgements

This work would have been impossible to accomplish without the help of so many people, and words cannot possibly describe how grateful I am to each and every one of them.

I would like to thank Prof. Dr. Pedro Baptista, who welcomed me into his lab with open arms, and guided me throughout this project. This has been the biggest challenge, but also the biggest opportunity of my life, and for that I thank you. Similarly, I would like to thank Prof. Dr. Cláudia Lobato da Silva for her assertive guidance 'from afar'. Without her, this thesis would not be possible.

I would also like to thank those who helped me in my daily endeavours. Here, I would like to particularly thank my lab colleagues, who were restless in helping me and providing the best company I could ever wish for. Thus, there are 3 particularly influential people who i would like to name. Sergio, who was my closest colleague during the development of this work, and to whom I probably owe my mental sanity after those long nights working in the lab; Sandra, the 'Portuguese-iest' Spanish person I know, who taught me everything about bioreactors and helped me every step of the way; And finally, Maria Jesús, the best lab technician I have ever met, who always goes the extra mile in helping each and every one of us. To these three people, and to all of the other colleagues who made me love the laboratory so much, I thank from the bottom of my heart.

There are also a number of people to thank who are not from the academic field. First and foremost, I am immensely grateful for my family, who have always supported me, and have thus allowed me to take the first big and small steps towards achieving my dream of doing science for a living. Here, my closest family takes on a central role. Even far away, they were always close, and never ceased to show their love and deep care for me. Thank you so, so much.

I would also not be here without the support of my girlfriend, Susana. This single, all-around amazing person has been a true rock for me, going above and beyond to show me how much she believes in me. She has always been my number one fan, and has never stopped cheering for me.

To my oldest friends, a perfect example of true comradery, and who I have known for over a decade now, I say: ours is the victory! To my newest ones, who have accompanied me in the last 5 years in this journey through college, and have shown me that short friendships can be just as strong as long ones, I also thank with my fullest heart. To all, thank you so much for these last 5 years. What an amazing ride it was.

Declaration

I declare that this document is an original work of my own authorship and that it fulfills all the requirements of the Code of Conduct and Good Practices of the Universidade de Lisboa.

Abstract

Liver disease is a global public health issue that affects from 4.5% to up to 9.5% people worldwide. The only current definitive therapy for end-stage liver disease is liver transplant - however, the demand for organ donors far exceeds their supply. Thus, a pressing need arises for accurate liver models that allow for better understanding of liver behaviour in health and disease. The present work lays the foundation for the development of vascularized liver organoid and liver tumouroid models by creating a microfluidic culture system in which human umbilical vein endothelial cells (hUVECs) and human mesenchymal stromal cells (hMSCs) are co-cultured with liver organoids or liver tumouroids in a three-dimensional microfluidic environment, supported by a fibrin hydrogel based on pig liver extracellular matrix (ECM). Co-culture of hUVECs and hMSCs in the absence of liver structures led to *de novo* formation of a microvascular network inside the microfluidic device. Angiogenesis was found to be caused by a combination of adequate cell conditioning and culture architecture, as well as by action of the ECM-based hydrogel. Improvements in experimental design are likely to allow for fruitful angiogenic assays in the presence of liver organoids or tumouroids. Furthermore, future applications of this technology include spheroid vascularization, high-throughput screening assays, *in vivo* modelling of human liver and other therapeutic approaches.

Keywords: Liver model, Liver organoids, Extracellulat matrix hydrogel, Microfluidics, Vascularization, 3D culture

Resumo

As doenças do fígado são um problema de saúde pública que afeta entre 4.5% e 9.5% da população mundial. Atualmente, o único tratamento definitivo no tratamento destas doenças é o transplante hepático. Contudo, a procura de dadores de órgãos é largamente superior à sua oferta, salientando a necessidade imperativa de modelos preditivos do comportamento de fígado, tanto em estado de doença como de saúde. O presente trabalho prepara o desenvolvimento de modelos de organoides e tumoroides hepáticos através da criação de um sistema no qual células endoteliais de veia umbilical humana (CEVUHs) e células estromais mesenquimais humanas (CEMHs) são co cultivadas com organoides ou tumoroides de fígado num ambiente tridimensional de microfluídica, apoiadas por um hidrogel de fibrina baseado em matriz extracelular de fígado porcino. CEVUHs e CEMHs co cultivadas na ausência de estruturas hepáticas levaram à formação de uma rede microvascular dentro do dispositivo de microfluídica. A angiogénese foi atribuída a uma combinação de condicionamento celular e arquitetura de cultura adequados, bem como à ação do hidrogel de matriz extracelular. É expectável que melhorias na conceção do sistema aqui relatado sejam suficientes para provocar angiogénese em co culturas de CEVUHs e CEMHs na presença de estruturas hepáticas. Aplicações desta tecnologia num futuro próximo incluem a vascularização de esferoides de fígado, ensaios de triagem de alto rendimento, modelos de fígado humano *in vivo* e abordagens terapêuticas.

Palavras-Chave: Modelo de fígado, Organoides de fígado, Hidrogel de matriz extracelular, Microfluídica, Vascularização, Cultura 3D

Contents

List of Figures

List of Tables

List of Acronyms

2D	two-dimensional
3D	three-dimensional
A230	Absorbance at 230 nm
A260	Absorbance at 260 nm
A280	Absorbance at 280 nm
ADMET	absorption, distribution, metabolism, excretion and toxicology
BCA	bicinchoninic acid assay
BSA	bovine serum albumin
BCLC	Barcelona Clinic Liver Cancer
chol-org	cholangiocyte-derived organoid
Col I	collagen type I
dECM	decellularized extracellular matrix
dh_2o	distilled water
DILI	drug-induced liver injury
DMEM HG	DMEM high glucose/Dulbecco's Modified Eagle Medium high glucose
DMSO	dimethylsulfoxide
ECM	extracellular matrix
EGF	epidermal growth factor
ESC	embryonic stem cell
FBS	fetal bovine serum
FDA	(U.S.) Food & Drug Administration
FGF	fibroblast growth factor
FITC-dextran	fluorescein isothiocyanate–dextran
GLX	GlutaMAX™
GMP	good manufacturing practices
HA	hyaluronic acid
HBV	hepatitis B virus
HCC	hepatocellular carcinoma
HCV	hepatitis C virus

hep-orgs	hepatocyte-derived organoids
I3A	Instituto Universitario de Investigación en Ingenería de Aragón
iPSC	induced pluripotent stem cell
INA	Instituto de Nanociencia de Aragón
LGR5	Leucine Rich Repeat Containing G Protein-Coupled Receptor
LoC	liver-on-chip/liver-on-a-chip
hMSC/MSC	(human) mesenchymal stromal cell
hUVEC	human umbilical vein endothelian cell
IGF	insulin-like growth factor 1
NAFLD	non-alcoholic fatty liver disease
PBS	phosphate buffer saline
PCR	polymerase chain reaction
PDL	poly-D-lysine
PDMS	polydimethylsiloxane
PFA	paraformaldehyde
PHEMA	polyhydroxyethylmethacrylate
PHH	primary human hepatocyte
P/S	penicillin/streptomycin
TXA	tranexamic acid
VEGF	vascular endothelial growth factor
WGO	World Gastroenterology Organisation

Chapter 1

Introduction

1.1 Problem statement and Motivation

According to the World Gastroenterology Organisation (WGO), over fifty million adults are estimated to suffer from chronic liver disease [1]. Furthermore, it is estimated that liver cirrhosis affects from 4.5% to up to 9.5% of the general global population [2, 3], while hepatocellular carcinoma affects over half a million people per year, and has a 5 year survival rate of 10% [1]. It was reported that, in 2015, cirrhosis accounted for 1.16 million deaths, while liver cancer accounted for 788,000 deaths, which means that liver disease-related deaths represented at least 3.5% of all deaths worldwide. These numbers, however, do not consider deaths resulting from acute hepatitis (145,000) nor those resulting from alcohol-use disorders (129,000), which elevate the number of liver disease-related deaths up to over 2 million deaths per year [4]. Due to the rise in the frequency of risk factors, such as diabetes, obesity, drug consumption, viral hepatitis, and alcohol consumption, these numbers are expected to grow in the near future [1, 4]. Indeed, in 2015 cirrhosis and liver cancer were respectively the 11th and 16th most common causes of death, while in 2000 they took the 13th and 20th places on that list, respectively [4]. Asrani, Devarbhavi and colleagues further report that this pattern of increasing mortality is also expected to grow, as incidence rates are also climbing; and in an even more concerning matter, these data are most likely underestimations, since liver disease often remains undiagnosed and is often disregarded as a cause of death.

Besides the great human cost discussed above, the socioeconomical burden of liver disease cannot be disregarded. The WGO reports that each North American cirrhotic patient costs approximately $4700 per year, almost twice as much as age-corrected non-cirrhotic individuals [5]. Older studies, pertaining to 2003, reported that total expenditure on chronic liver disease and cirrhosis, chronic hepatitis C and liver cancer in the U.S. surpassed $3.5 billion in 1998 [6]. More up-to-date figures from 2015 show that the treatment of patients with hepatitis was the most costly among all gastrointestinal tract-related treatments in the U.S., being associated with a direct burden of $23.301 billion [7]. The study further reports that, in that same year, over $38 billion were spent in the treatment of non-cancerous liver and gallbladder diseases in the U.S.A.. Furthermore, liver disease in the U.S. is heavily correlated with several other socioeconomic conditions, such as unemployment, disability rates of unemployed individuals, global

healthcare expenditures in liver disease patients and general loss of quality of life [8]. Across the world, in South Korea, a 2011 study reported that, between 2004 and 2008, yearly socioeconomic costs of liver disease fluctuated between KRW 5 572 billion (roughly $4.713 billion) and KRW 8 104 billion (roughly $6.847 billion), representing as much as 0.62% of the country's GDP [9, 10]. Although the staggering increase in costs seen in the U.S. may simply be due to more reported cases and better understanding of liver pathology, the sheer magnitude of these numbers nonetheless represents a rather worrying reality. The prevalence and associated cost of liver disease can not be ignored, and should be addressed immediately.

To address liver disease, one must understand normal liver behaviour, as well as liver pathology and the interaction of the liver with drugs. For these purposes, a multitude of models can be employed, ranging from computational simulations to *in vivo* models of mice, minipigs, and other animals, which are inaccurate due to interspecies variation between them and humans [11, 12]. Another route pursued by some groups is that of liver-on-a-chip devices [13]. However, none of these models are an exact representation of the human liver [13, 14]. Thus, the need arises for a model that can accurately portrait human liver function in as many scenarios as possible. Ideally, the model of a liver would be another liver - which clearly is not viable for high-throughput, replicable science, given the organ's indispensable nature to the human body. A promising alternative is presented in the form of liver organoids, small structures that recapitulate the function of liver parenchyma. However, like most human-based models, and unlike the liver, organoids are typically avascular structures. Therefore, adequate vascularization of liver models might just be the next key step towards improving said models, since it would allow for near-physiological nutrient, metabolite, and gas exchanges between the model and the circulating fluid.

1.2 Liver, liver pathologies and state-of-the-art solutions

The liver is the largest gland of the body, weighting around 1.5kg in adults, and is the metabolic centre of the body. It is divided into two lobes, right and left, with the former being larger than the latter, and further subdivided into lobules [15]. In itself, the liver carries the majority of the weight when it comes to the primary detoxification of a multitude of metabolites, protein synthesis and the production of digestive enzymes, while simultaneously regulating red blood cells and glucose synthesis (via gluconeogenesis and glycogenolysis) and storage [16, 17]. Regarding metabolism *per se*, the liver takes on an enormous role in breaking down digestion products, via the aforementioned digestive enzymes, and drug components. A normally functional liver processes the entire blood every four minutes [17].

1.2.1 Liver histology

Liver lobules, which are the organ's functional unit, are roughly hexagonal structures where each corner is defined by a complex known as a portal triad, which is comprised of a portal vein, a hepatic artery and a bile duct (Figure 1.1a) [18]. The lobule itself is made up of hepatocytes, which are considered to be subdivided into 3 zones, based on function and perfusion (Figure 1.1b). Zone I is highly perfused

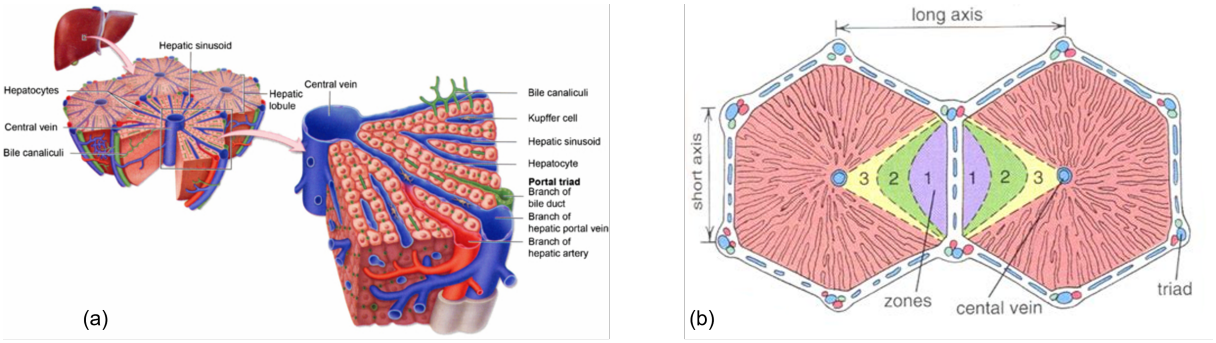

Figure 1.1: (a) - Schematic representation of liver, with division into lobules (right) and a further detailed look into liver microvasculature (left), as depicted by Stenvall *et al.* [20]; (b) - Characterisation of lobule hepatocytes by zones, from most perfused (zone I) to least perfused (zone III) [21].

and oxygenated, since it is the closest to the portal vein; therefore, this is a highly metabolic area, playing a key part in gluconeogenesis and cholesterol regulation, as well as beta-oxidation of fatty acids and the formation of bile. Zone II is an intermediate area, where hepatocyte function gradually changes from that seen in zone I to that of zone III. Zone III is thus the furthest away from the portal triad, where the roles of glycolysis, ketogenesis, lipogenesis, glutamine formation and glycogen synthesis are taken on. Furthermore, zone III is also highly responsible for the biotransformation of drugs and the detoxification of the blood [18].

Bile caniculi, formed by the apical membrane of hepatocytes, facilitate bile flow in a countercurrent direction relative to the blood, from zone I to zone III [19]. Fenestrated capillaries in the liver sinusoids facilitate irrigation of the lobule, draining blood into the central vein, which is in turn a branch of the hepatic vein. Lastly, the area occupied by microvilli from the basolateral membrane of hepatocytes is called the space of Disse, which separates the cell body from the blood vessels while maximizing the area of contact between the microvilli and the blood. In this area, hepatocytes are vascularized by the capillaries in an ECM-rich environment composed of various types of collagen molecules and proteoglycans. The space of Disse also houses Kupffer cells, the immune cells of the liver, and stellate cells, which store fat and support liver regeneration [19].

1.2.2 Liver pathology and current treatment

With a global death toll of over 2 million people per year, liver disease commonly presents itself in the form liver failure or as liver cancer [4]. Incidence rates of various types of diseases are not homogeneously distributed among regions, wealth levels, and ethnicities. Nevertheless, all populations show some sort of generalized prevalence of at least one type of liver disease, making it a generalized, global issue.

1.2.3 Liver cancer

Liver cancer describes any cancer that has its origin in the liver [22], of which over 80% are hepatocellular carcinomas (HCCs), with the remainder of cases being intrahepatic cholangiocarcinomas (roughly 6% of all liver cancers) [23], angiosarcomas and hemangiosarcomas (0.1%-2% of all primary liver cancers)

[24], and very rarely hepatoblastomas, which affecttheirits high prevalence. With over 810.000 deaths per year, it is the 2nd and 6th most common cause of cancer deaths in men and women, respectively [4]. Furthermore, HCC has the second worst survival rate among cancers, with a 5-year survival rate of 18%. Main causes of HCC are hepatitis B virus (HBV) infection, hepatitis C virus (HCV) infection and alcohol consumption. HBV and HCV infection collectively account for 60%-85% of HCC cases, besides being prominent risk factors for other sources of HCC, while the consumption of more than 80g of alcohol represents a 5-fold increased risk of HCC. Besides HBV and HCV, risk factors for HCC include cirrhosis, fatty liver disease, diabetes and alcohol. Current trends in the increase of life expectancy, but also of obesity and diabetes are expected to cause an increase in HCC incidence, unless preventive measures are adopted, such as anti-HBV and anti-HCV vaccinations and switching to an overall healthier lifestyle [4].

The treatment of HCC is a very challenging decision-making process, which must take into account the patient, the progression of the disease and the severity of liver dysfunction, as well as the available resources. In an earlier stage, HCC can be treated with surgical resection when the patient shows no signs of portal hypertension and an adequate classification on the Barcelona Clinic Liver Cancer (BCLC) staging classification, although recurrent HCC is developed post-resection in 70% of the patients [25]. Transarterial embolization (chemotherapy)+radiotherapy and ablation treatments are also available, as well as systemic pharmacologic treatments. In the end, however, the most definitive option for the treatment of HCC is liver transplantation, removing both the tumour and the impaired liver. The great drawbacks of this therapeutic approach are the lack of donors, since a complex list of requirements must be met for liver donation and the liver is an essential organ, and the requirement of lifelong immunosuppression of the patient [25].

1.2.4 Cirrhosis

Cirrhosis is "the histological development of regenerative nodules surrounded by fibrous bands in response to chronic liver injury, that leads to portal hypertension and end stage liver disease" [26]. This fibrotic mechanism is caused by a perpetuation of an inflammatory response, which ultimately leads to the generation of non-functional scar tissue through the deposition of connective tissue around the liver parenchyma, especially in the space of Disse. This, in turn, leads to blood being shunted away from hepatocytes, rendering them unable to perform their regular blood-filtering function. Ultimately, cirrhosis can lead to several complications, like spontaneous bacterial peritonitis, encephalopathy and liver failure [26]. Cirrhosis is often the culmination of the development of one or multiple liver diseases, which can be caused by viral agents, such as HBV and HCV, or non-viral agents, which is the case in non-alcoholic fatty liver disease (NAFLD) and in alcohol-associated liver disease.

The progression of cirrhosis can be divided into two stages, namely compensated and decompensated cirrhosis. As hinted at by the name, in compensated cirrhosis the body is still able to adapt to the irregularly functioning liver. Although compensated cirrhosis goes mostly undetected, the patient may have non life-threatening symptoms of the disease. The transition to decompensated cirrhosis occurs when the

patient develops more dramatic complications, like variceal hemorrhage, ascites or the aforementioned spontaneous bacterial peritonitis and hepatic encephalopathy. In its decompensated stage, the disease is much less manageable, and treatments are often less effective [26].

Treatment of cirrhosis is initially carried out by eliminating its cause. For example, in alcoholic cirrhosis, alcohol consumption must be avoided, whereas some cases of HCV-induced cirrhosis benefit from antiviral treatment [27]. In HBV-derived cirrhosis, some orally administered treatments can even fully prevent effects from the end stage of the disease [28, 29]. However, should these preliminary approaches fail, the only treatment available to effectively cure cirrhosis is liver transplant, which in 2019 had a one year survival rate of 90% and a 5 year survival rate of 73% [30]. Nevertheless, recurring infections after liver transplant are not uncommon, especially in HCV-induced cirrhosis [26].

1.2.5 Liver transplantation

As seen, liver transplantation remains the only available definitive treatment for liver failure. It is the second most common solid organ transplantation, comprising 22% of all solid organ transplantations, after kidney, which represents 65% of all solid organ transplants [31]. Twenty-one percent of liver transplantations are from living donors, a paradigm which is more common in Asia than in Western countries [4].

Facing global donor shortages, measures to increase the number of available organs, such as the 'brain death law', which was adopted in most Asian countries [4], are continuously being studied and considered. Many countries have implemented measures such as loosening the criteria for organ suitability, allowing for donations after circulatory death and 'opt-out' systems for organ donation, instead of 'opt-in' [4]. In the particular case of Spain, one of the worldwide leaders in the number of liver transplants, with over 40 donor per million inhabitants as of 2016, additional policies were carried out in which possible donors are identified early and encouraged to donate [32]. Furthermore, non-standard donors (older or at-risk individuals with localized malignancies) are also considered as a valid source for donations. Lastly, an investment was made in the development of infrastructures that facilitate easier and quicker liver donation [32]. As for the host of the liver transplant, they are initially classified according to the model for end-stage liver disease (MELD) to evaluate eligibility and need for transplantation and, upon transplant, must be kept under immunosuppresion, so as to not reject the donated organ [33]. Even so, the effort is still insufficient to meet the high demand for liver transplantation, as 2.7% of Spanish patients still died in 2019 while on the waiting list for liver transplant, according to the Spanish National Transplant Organization.

1.2.6 Drug components and their interaction with the liver

Drug metabolism

As previously stated, key functions of the liver include drug metabolism. This process occurs mainly through biotransformation, although some drugs are metabolized with the aid of lysosomes. Biotransformation spans over 2 phases and aims at transforming xenobiotics by converting them into a hydrophilic form [19]. In phase I of this process, the xenobiotics undergo oxidation, reduction and hydrolysis, mainly by

enzymes of the cytochrome P450 family, which prepare the drug for phase II. Phase II reactions conjugate the results of phase I to hydrophilic glucuronate, glutathione or sulfate groups, which can be secreted into the blood or bile [19]. One crucial factor to take into account is that, for its conjugation, glutathione must be reduced - however, the depletion of reduced glutathione causes toxic metabolites to build up.

Drug toxicity

Indeed, although the great majority of approved drugs is mostly beneficial for patients, providing adequate care a specific pathology, many of them, including drugs used in daily practice, often have unintended side effects that end up weighing heavily on the liver [34]. In fact, roughly 50% of candidate drugs present undesired effects on the liver, causing frequent regulatory measures and drug withdrawal [35]. Drug-induced liver injury (DILI), which commonly leads to liver transplantation, affects 14-19 per 100.000 people, with severity and incidence depending on the drugs that cause it, among other factors. DILI can be dose-dependent (intrinsic), which we can predict, or, more commonly, dose-independent (idiosyncratic) [36], although it has been shown that a paradigm of inflammation can heavily reduce the differences between one case and the other [35].

In a nutshell, DILI occurs when local tissue inflammation and the aforementioned toxic metabolites that result from drug processing cannot be hampered by the body's immune system nor cleared away sufficiently fast [35]. Idiosyncratic DILI is heavily host-dependent, which means that risk factors such as age, gender, co-medication, underlying conditions, key polymorphisms and even gut microbiome play a role in determining how big the damage will be [35]. Some key drug properties to keep in mind regarding drug-induced liver injury are the threshold dose, the lipophilicity of the drug, its formation of reactive metabolites, the oxidative stress caused by the drug, the mitochondrial liability that the drug presents and the inhibition of hepatobiliary transporters by the drug.

For these instances, it becomes evident that the scientific community and the pharmaceutical industry are in dire need of sustainable and accurate liver models that can produce physiologically relevant results by accurately replicating the *in vivo* behaviour of the liver in an *in vitro* setting. Currently, 2-dimensional cell cultures have been employed for that effect, but with insufficient results. Robust, *in vivo*-like models are needed to fill this gap.

1.2.7 State of the art in liver models

The liver is a highly complex organ with intricate cell-to-cell interactions which enable it to adequately perform its functions [37]. Thus, an appropriate liver model should be able to replicate or simulate these very interactions, in order to get as close as possible to a representation of a real liver. In this scenario, one can consider human models or animal models. Despite being more easily available, being capable of providing a general idea of liver mechanisms and behaviour, and offering the possibility for an easier organism-wide study of disease pathology and etiology, animal models are not capable of accurately representing human liver. Even with all of the advances made with mouse-, rat- and minipig models [11, 14], for instance, discovery mainly focused on human-based systems is the next great step in liver

Table 1.1: Comparison of different cell sources for 2D culture liver modeling regarding cost, availability, proliferation, lifespan and liver phenotype markers.

	PHH	HepG2	HepaRG	iPSC
Cost	High	Low	Mid	High
Availability	Very low	High	High	High
Proliferation \textit{in vitro}	Low	High	Mid	Theoretically unlimited
Lifespan	Short	Immortalized cells	Differentiation steps	Differentiation steps
Albumin release	High	Low	Mid	High
Drug response	High	Low	Mid	Mid
CYP expression	High	Low	Mid	Mid

modeling, especially if the aim is to obtain results that can be translated into clinical practice [14]. Typically, liver models can be categorized into two-dimensional (2D) cell cultures, three-dimensional (3D) cell cultures and liver-on-chip models, each with their advantages and drawbacks over the others, although some models are hybrids between two of these categories.

2D cell culture models

Over the course of the last 4 decades, ADMET (absorption, distribution, metabolism, excretion and toxicology) mechanisms of prospective drugs have been analysed through *in vitro* essays performed on hepatocytes, in an attempt to predict liver damage and the effect of the drug on the body [38]. In this scenario, primary human hepatocytes are considered the 'gold standard', and have been thoroughly studied in what regards their isolation, *in vitro* behaviour and pharmacokinetics [39].

Primary human hepatocytes (PHHs), however, are not widely available, requiring a great monetary and time investment for their isolation from human tissue. Thus, alternative cell sources arise in the form of HepG2 cells, an immortalized cell line derived from a well-differentiated hepatocellular carcinoma, or HepaRG cells, isolated from a liver tumour of an HCV-infected patient [37]. Yet another alternative cell source can be found in induced pluripotent stem cells (iPSCs), which can be differentiated into liver cells[37]. Pros and cons of these cell types are detailed comparatively in Table1.1. As can be seen, cells with higher fidelity to *in vivo* liver behaviour, shown by the expression of enzymes from the cytochrome P450 family, albumin production, and drug response, are more costly and vulnerable, while established cell lines typically require less maintenance, but also yield poorer results. Furthermore, being from established cell lines, HepG2 and HepaRG cells, unlike PHHs, have a fixed phenotype, failing to represent the adapting nature of liver hepatocytes.

A major innovation in two-dimensional cell culture has been the integration of the so called 'sandwich' culturing method, with the purpose of extending the lifespan of cultured cells [40]. In sandwich cultures, the cells are seeded on a layer of ECM proteins, but are also covered by another protean layer, providing a stable culture scaffold and incentivizing cell-cell interactions. PHHs cultured in such systems typically display a defined three-dimensional shape and polarity, with defined apical and basolateral domains [40].

3D cell culture models

Despite the advancements seen in 2D cell culturing techniques, and the current research trying to optimize two-dimensional culture methods, mono-layer cultures are inherently flawed in that they do not accurately represent three-dimensional liver architecture, especially due to the absence of hepatocyte polarity in 2D culture, which causes them to enter a dedifferentiation process [37]. Thus, 3D alternatives were sought to increase the accuracy of liver models.

Initially, attempts were made to produce 3D hepatocyte spheroids by self-aggregation upon culture on an ultra-low attachment plate or by embedding hepatocytes in an ECM-like hydrogel [41]. These attempts generated spheroids composed of well-defined, well-polarized hepatocytes with meaningful cell-cell interactions. In comparing PHH spheroids with their 2D counterparts, proteomic and transcriptomic analyses found that three-dimensionality induces a phenotype which resembles that of native liver [42]. Additionally, basic liver functions, such as albumin secretion and glycogen storage were preserved for up to 5 weeks. ADMET studies also attest to the improvements brought on by spheroids, which showed more sensitivity to acetaminophen or amiodarone when compared to 2D sandwich cultures [38].

However, the liver is not only made up of parenchymal cells. Therefore, if a realistic model is to be made, other cell types, like Kupffer cells, endothelial cells or cholangiocytes, which all play a key part in liver functions, must also be included [38]. Thus, co-cultures of hepatocytes and non-parenchymal cells are currently being investigated with promising results [37]. Another current direction being explored is that of liver organoids, a specific type of self-enclosed spheroid structures that aim to recapitulate liver behaviour. These will be discussed in more detail in subsection 1.2.8.

Liver-on-chip models

Liver-on-chip (LoC) or liver-on-a-chip models are a subclass of the so-called 'organ-on-chip' models that hinge on the concept of microfluidics (which will be explored further in section 1.3.3) to accurately represent the liver [43]. In a nutshell, microfluidics is an attempt at providing a high degree of control over the culture system by reducing its size and the volume of the liquid that flows through it. In doing so, parameters such as flow rate and pressure of the circulating fluid become more controllable, and a higher degree of homogeneity is ensured.

LoC devices rely on seeding hepatic cells (in mono-culture or co-culture) on a surface that is dynamically perfused with medium, functioning as a makeshift hepatic sinusoid [43]. The versatility of LoC devices has successfully been exploited to model liver architecture, zonation of liver hepatocytes, and liver disease [37] (like NAFLD and HBV), so much so that a commercial LoC, LiverChip® , has already been developed and commercialized by CN Bio Innovations (UK). However, especially in the case of disease modeling, the LoC devices are very goal-oriented, being specifically manufactured with the purpose of modeling that specific disease [37]. Thus, there is still a gap to be filled in the development of a universal liver model applicable to most situations.

1.2.8 Liver organoids

Organoids are the result of over one century of attempts to grow functional tissue *in vitro*. In their simplest form, they are three-dimensional cell structures that resemble the function of a specific tissue, although it is not uncommon for them to simulate the tissue's anatomy and cellular composition as well. These structures are typically made by self-organization of progenitor cells into spheroids that show a tissue-specific behaviour, either from being isolated from said tissue or from being differentiated into the desired cell type. The former is the case of adult-derived progenitor/stem cells, or primary cells, while the latter is typically associated with pluripotent stem cells, which can be embryonic stem cells (ESCs) or iPSCs [44]. Organoids are particularly interesting in that, through their recapitulation of the organ's behaviour, combined with their small size, they allow for a down-scaled predictive model for organ response that has the potential for mass production, while being contained in a lab under any desired conditions [44]. This phenomenon allows for accurate modeling while bypassing (or significantly diminishing) the need for live tissue samples, minimizing the number of transplant-valid organs that have to be donated to science. Organoids are characterized by their self-renewal throughout prolonged periods, their clonal expansion capacity, and their multipotency [44]. Sometimes, the term 'organoid' is also employed to refer to any tissue-derived 3D structure that is kept in culture, although this, unless stated otherwise, will not be the case for this work.

The generation and maintenance of self-assembled organoids is a laborious process which includes the isolation of the cells from a tissue (embryo for ESCs, the target tissue for primary cells, and multiple sources for iPSC precursors, which then have to be reprogrammed into iPSCs) and the plating of those cells into a 3D substrate that resembles the native ECM of the target tissue (traditionally Matrigel™, a matrix rich in laminin and collagen IV derived from Engelbreth-Holm-Swarm tumours) [45]. Then follows the conditioning of the cell culture with medium supplemented by the appropriate growth factors to differentiate the cells into the desired fate, if they are pluripotent, and to inhibit apoptosis and differentiation pathways, while stimulating the activation of migration and proliferation pathways, facilitating organoid generation [44].

One of those growth factors is r-spondin, which, *in vivo*, is secreted by stem cell niches. When artificially introduced in a conditioning environment, r-spondin can help regulate the Wnt pathway by binding to the LGR5 receptor of the cells, triggering a cascade that ultimately stops the destruction of β-catenin, a crucial transcription factor in the pathway. β-catenin then binds to TCF, transcriptional co-activators that enable the expression of Wnt-related genes, which themselves promote the self-renewal of stem cells, a defining element of organoid culture [46, 47].

Previously, organoids had been associated with the ethical dilemmas that come from harvesting embryonic cells. However, these barriers have been mostly overcome, due to the generation of organoids from iPSCs or primary cells. Furthermore, organoids seem to have very promising applications in the fields of drug discovery, clinical practice and tissue engineering/regenerative medicine: while their potential for high throughput assays, combined with their accurate modeling, is particularly enticing to pharmaceutical companies for drug screening studies, the field of personalized medicine is exploring the generation of patient-specific organoids, which would enable a personalized treatment plan for every patient [44].

This is particularly interesting in the treatment of malignancies, due to their high genetic and behavioural variability. Regarding regenerative medicine, some proof-of-concept studies have been carried out in which organoids were transplanted onto mice, retaining their function and histology [48].

Fabrication of liver organoids

Adult stem cell-based liver organoids Initially, liver organoids were obtained by the previously described r-spondin-based conditioning of LGR5+ cells [49]. These organoids exhibited bipotency by expressing markers characteristic for hepatocytes, but also for bile duct, showed hepatic karyotype and function, and were maintained in culture up to several months. The same principles, but a slightly changed protocol, allowed for the assembly of the first 3D human liver organoids 2 years later [50]. Here, TGFβ inhibition was found to be necessary for the generation of liver organoids, alongside Wnt stimulation. These organoids were also found to retain disease phenotypes from their donors. Further refining of this protocol led to the production of cholangiocyte-derived organoids (chol-orgs) and hepatocyte-derived organoids (hep-orgs), with the latter emulating a phenotype characteristic to post-resection hepatocytes, showing expression of albumin, Hnf4α, Cyp1a2 and Cyp3a11, as well as secretion of albumin [51]. Recent developments show that adequate medium perfusion also has an influence in organoid behaviour. Upon having been cultured in spinner flasks, human liver organoids presented larger size and higher growth rates than organoids grown in a typical 3D culture, possibly because of the higher amount of oxygen being delivered to the cells [51].

Pluripotent stem cell-based liver organoids The first instance of liver organoids from a pluripotent cell source happened in 2013, when iPSC cells were committed to an endodermic fate and co-cultured with hUVECs and hMSCs to form a three-dimensional, iPSC-derived liver bud. The resulting structure proved to be transplantable into immunocompromised mice, connecting to the host's blood vessels and secreting albumin into their blood stream [52]. The protocol was later refined to be in accordance with good manufacturing practices (GMP) without affecting engraftment ability. Paracrine signaling also appears to play a role in the formation and maintenance of liver organoids, and cell-cell contact between parenchymal and non-parenchymal cells was shown to be essential for the generation of three-dimensional structures, further emphasizing the role of stromal cells in liver organoid cultures [53]. A recent study took on a novel approach, gradually differentiating pluripotent cells as though they were passing through embryonic organogenesis [54]. Hepatic organoids formed by this method contained sheets of hepatocytes, as well as cholangiocytes surrounding structures that resemble bile ducts. Furthermore, these organoids showed regenerative properties and the ability to generate secondary organoids.

One last important note about liver organoid production regards the reliance on xenogeneic materials during the culturing process. Matrigel® is widely used as a substrate for three-dimensional cell culturing due to the high level of support it provides, both mechanically and regarding protein activity. However, it is highly subject to batch-to-batch variation, negatively affecting the reproducibility of the organoids embedded in it, and is also not suitable for clinical practice [55]. Thus, xeno-free solutions have been developed in the forms of a polyethylene glycol hydrogel and a polyisocyanopeptide hydrogel, although

the latter has found less success than the former [56, 57].

Liver organoids in disease modeling

Organoids are particularly interesting for disease modeling, since not only do they simulate the behaviour of the liver, but they do so while retaining the genetic and phenotypical characteristics of the donor. Thus, it is now possible to conduct large-scale, high throughput essays to study the mechanisms of specific diseases without requiring a large amount of patients [58]. Furthermore, this phenomenon opens the door to personalized medicine, a paradigm in which each patient is treated in a custom manner, according to their genetic and drug response profiles, avoiding waste and elevating treatment effectiveness, providing that the disease itself is not a hurdle for organoid formation. Additionally, patient-derived organoids can be used to form a biobank of liver disease and, through the help of genome modifying technologies like CRISPR/Cas9, the genetics of the organoid can be altered to induce or cure a disease [58].

Monogeneic diseases Diseases such as Alagille syndrome, α-1 antitrypsin deficiency, cystic fibrosis and Wilson's disease are monogeneic diseases that originate and/or have high repercussions on the liver [58]. Being genetic disorders, patient-derived organoids can offer a way for *ex vivo* modeling of the disease [50, 59]. Models of Alagille syndrome and α-1 antitrypsin deficiency have already been made, further helping the characterization of these pathologies. Notably, in the case of Alagille syndrome, it was possible to revert the disease by gene editing, restoring damaged hepatic structures to their regular form [59]. Models for cystic fibrosis and Wilson's disease have not yet been developed, although a similar pattern of improvement to the characterization of the pathologies is expected for these diseases.

Steatohepatitis Steatohepatitis is a type of fatty liver disease which showcases liver inflammation and accumulation of fat in the liver [60]. In order to model the disease, Ouchi and colleagues devised liver organoids made up of iPSC-derived hepatocyte-, Kupffer-, and stellate-like cells, which were functional, as confirmed by cytochrome P450 activity, LPS response, and vitamin A storage, respectively [61]. Treatment of these organoids with oleic acid resulted in a dose-dependent lipid accumulation, as well as inflammation. The same group made a 3D model of Wolman's disease from patient-isolated iPSCs, which, when treated with FGF19, hampering the disease's phenotype [62]. Alcoholic steatohepatitis has also been modeled, with organoids derived from embryonic stem cells in co-culture with human fetal liver mesenchymal cells that were treated with ethanol, resulting in the disease's characteristic phenotype [63].

Viral hepatitis Infection by HBV and HCV still remains a prevalent problem at a global scale. Having been extensively characterized, these viral diseases are prone to being modeled by liver organoids [58]. In fact, iPSC-based organoids have been developed that were susceptible to HBV infection [64], a feat that was not possible in hepatoma cell lines due to the absence of sodium-taurocholate cotransporting peptide, an HBV entry factor. However, this model was developed with non-human cells, meaning that the gap for HBV- and HCV-infectable human organoids is yet to be bridged.

Primary liver cancer Currently, primary liver cancer is most effectively modeled by transplanting patient-derived xenografts onto immunocompromised mice [65], since 2-dimensional cultures did not yield accurate results, and did not present the heterogenicity characteristic of *in vivo* HCCs [58, 66]. Even so, xenografts on mice models are too labour- and time-intensive to provide high-throughput screening platforms, and are missing immune cells, which are key to understanding the generalized systemic response to the carcinoma [67].

Organoids represent a promising modeling approach for primary liver cancer in that they combine the advantages of 2D cell culture and xenograph models, with the additional perk of being able to generate patient-specific tumour models. So far, primary liver cancer organoids have been successfully derived from human patients and from mice, through surgical resection [68]. To avoid biases introduced by surgical resection, HCC and cholangiocarcinoma organoids can be generated from tumour tissue harvested through needle-biopsy. However, it is important to note that these methods have low efficiency rates, as only 26% of biopsy-derived organoid attempts led to a successful outcome, while the same happened for only 27% of resection-derived organoids [69, 70]. Nevertheless, the successful attempts were found to closely recapitulate the primary tumours' histology, attesting to the maintenance of phenotype in an *in vitro* setting. Furthermore, it was found that over 90% of the genetic alterations of the primary tumours were maintained, with only a small number of *de novo* mutations being observed, and that intratumour heterogeneity was maintained when compared to the biopsies [69, 70]. The latest novel approach has successfully explored the idea of creating cancer organoids by editing the genome of existing cholangiocyte organoids with CRISPR/Cas9 technology [71]. Transplantation of these organoids into mice originated xenografts with HCC or cholangiocarcinoma features, thus opening the door for another method of fabrication of liver cancer organoids.

One drawback of current protocols for the generation of cancer organoids hinges on the absence of other cell types in the tumour [58]. However, as previously shown, this can be easily overcome by co-culturing the 'tumouroids' with stromal cells of the liver, replicating adequate liver environment and cell-cell interactions. Furthermore, cancer organoids seem to respond to conventional cancer therapies, and can be cryopreserved to form a cancer organoid biobank.

1.3 Introduction to methodology

1.3.1 3D cell culture

The term cell culture refers to artificial cell expansion and maintenance in a controlled laboratory setting. For this, cells are placed inside a culture dish, flask or other culture surface and are generally immersed in cell type-specific medium which gives the cells the conditions and nutrients to grow and expand. Other parameters, such as oxygen percentage of environmental air, temperature and plate confluency also impact cell behaviour and growth. Another defining factor for cell behaviour is whether the culture surface has been treated. Specific compounds, such as collagen or gelatin, can potentiate cell adhesion [72, 73], while others (like those present in ultra-low attachment plates) can have the opposite

effect, inducing cells to remain in suspension, which can be useful to create cell aggregates [74].

Three-dimensional cell culture Although cell culture initially took place in a two-dimensional setting, the drive to try to mimic physiological systems *in vitro* led to the discovery of three-dimensional cell culture. 3D cell culture typically places a higher value on mechanical stimuli and spatial organization, as well as cell-cell and cell-matrix interactions, than classical 2D cell culture. This has a wide array of phenotypical repercussions in gene expression, cell morphology and sensitivity to drugs, among others [75]. Indeed, it has been shown that 3D cultures generally resemble *in vivo* cell and tissue behaviour more closely than 2D cultures, especially in non-barrier organs or tissues [76]. 3D co-culturing of different cell types is also particularly interesting, since cell-cell interactions in a 3D *in vitro* environment facilitate the formation of cellular niches that resemble those found in *in vivo* setting. The U.S. Food Drug Administration (FDA) reports that 3D cell culture devices for liver and heart are especially relevant, since these organs are the most frequent drug targets [77].

Three-dimensionality in a culture system can currently be achieved via 3 different methods: hydrogels, other scaffolds or scaffold-free techniques. While hydrogels will be further detailed in section 1.3.2, and scaffolds will be of less interest for this project, it is important to note that scaffold-free techniques include the hanging drop method, which was used in this work for the formation of HepG2 tumouroids. In this technique, drops of cells suspended in their culture medium are placed on the inside of an upside-down lid of a conventional Petri dish. The lid is then turned right side up and placed on top of its corresponding plate, which causes the drops to be pulled downwards by gravity. However, liquid tension keeps the drops attached to the surface of the plate. Gravity also acts upon the cells, causing them to converge to the middle of the drop. The cells then tend to aggregate, through cell-cell adhesion mechanisms, therefore effectively forming a three-dimensional structure [78].

1.3.2 Hydrogels

Hydrogels are three-dimensional, cross-linked polymeric structures which can retain a high amount of water without dissolving or losing their structural properties [79]. Having originally appeared in 1960 in the form of a bio-compatible polyhydroxyethylmethacrylate (PHEMA) gel, hydrogels have since evolved into finely tunable compounds from all kinds of sources that are able to carry out key roles roles in tissue engineering, as scaffolds, drug-delivery systems, and antifouling coatings, and in other areas, like the manufacturing of soft contact lenses, for instance [80, 81]. Gelation, the process of solidification of a hydrogel, consists of chemical or physical reactions that form cross-links between the polymer chains, creating a cohesive and structured three-dimensional network [79].

Hydrogels, especially those used in biomedical applications that imply direct contact with tissues, need to undergo rigorous examination in five key areas: physical (including swelling ratio, thermodynamics and porosity) , chemical (chemical composition and interactions), mechanical (response to mechanical stress, toughness, Young's modulus), rheological (loss/storage modulus, viscosity) and biological (biocompatibility, biodegradability and bioactivity) [79]. There are no universal optima for each of these parameters, since each hydrogel must be adapted to its purpose. For instance, shape retention and optical properties might

be important for a hydrogel-based contact lens, whereas the bigger concern for a hydrogel-based drug delivery system might be the biocompatibility, the bioactivity, or the porosity, which affect the release rate of the drug.

Regarding their mechanical properties, hydrogels are typically considered weak, as they have low fracture energy ($<10\ J\,m^{-2}$) and toughness, which limits their use in more demanding environments, such as artificial cartilage and soft robotics [82]. However, it is possible to toughen hydrogels through one of three types of toughening mechanisms: introducing mechanisms to dissipate mechanical energy and avoid crack propagation, increasing structural homogeneity, which hinders stress concentration, or a combination of both previously described mechanisms [79].

A sub-type of hydrogels are those with the "self-healing" property, in which they are able to heal damage caused to them without interference from other agents. This phenomenon is especially alluring in that these hydrogels are more durable and reliable in their behaviour than non-healing gels. Self-healing can be characterized as physical, where the hydrogel rebuilds the network via noncovalent, reversible interactions, or chemical, where the reassembly is done through covalent chemistry [79].

Hydrogels for Liver Tissue Engineering

Liver tissue engineering deals with the fabrication of structures, which, in some form or another, resemble the liver. Components of the native liver can be classified into different categories, namely the vascular system, the stroma, sinusoidal cells, hepatocytes and cholangiocytes, which have intricate interplay and form a complex, cohesive structure that enables the liver to perform its various functions [83]. However, fabricated liver tissue does not necessarily have to showcase the same level of complexity. Depending on the purpose of the generated structures, different approaches can be taken for an *in vitro* model of liver tissue, although, as previously seen, it is widely accepted that 3-dimensional structures add robustness to the model and are therefore preferred in most applications [84]. Indeed, one could say that, so long as the engineered tissue is similar to liver in mechanism and function, and the process was conducted with adequate diligence, any approach is valid.

One possible approach to strive for functional bioengineered liver tissue is to artificially recreate the extracellular matrix of the liver, in which cells or other relevant structures would then be embedded. In fact, it has already been proven that liver ECM, which is mainly concentrated in the space of Disse, plays a critical part in what regards cell polarization and gene expression and differentiation in the liver [84]. Cells in the liver lobule, having no basement membrane, are mostly supported by an ECM consisting of fibronectin and collagens (types I and III-VI), as well as of laminin, elastins, glycosaminoglycans, and proteoglycans, both in healthy and fibrotic liver (although fibrotic liver showcases much higher quantities of ECM) [85, 86]. In being fibrous, the scaffold at the backbone of liver ECM serves as a surface for cell adhesion, while simultaneously enabling cell growth and migration and interacting with progenitor cells [87]. The replication of all these functions of the liver ECM in a laboratory setting is not trivial, as it demands high control over some key biological, physical and chemical properties.

Biological properties The scope of biological properties is undoubtedly the most important one when the goal of the hydrogel is to help produce biologically functional liver tissue which, in itself, will also have living cells that interact with their surroundings. So, special care must be taken regarding the biocompatibility, biodegradability and bioactivity of the hydrogel [84]. Biocompatibility is crucial to ensure normal cell growth, behaviour, and migration patterns [88]. This can be achieved, for example, by avoiding cytotoxic materials or by treating the culturing surface of the hydrogel. Biodegradability, on the other hand, is interesting in what regards transplant approaches, since it enables a seamless incorporation of the hydrogel into the host's body [89]. In this case, the hydrogel would have to be built around the enzymes responsible for the degradation mechanisms present in the host-to-be. Lastly, bioactivity describes the behaviour of the hydrogel towards the cells, viewing the gel not only as a scaffold or a support system, but also as an active player in the regulation of cell behaviour through the transmission of environmental signals [90]. It plays a particularly significant role when the hydrogel contains some sort of chemical (for example, a drug) which is gradually delivered onto the cells or structures embedded in the gel.

Physical and chemical properties Properties such as mechanical stiffness, porosity, mechanical stress and mechanical strength, elasticity, swelling, and viscosity have also been seen to play a big role in cell growth and phenotype regulation [84]. More concretely, stiffness has been seen to directly influence cell behaviour [91], while pore size and porosity influence the delivery of nutrients, growth factors, and oxygen to the cells in culture [92]. Indeed, Desai *et al.* found that a matrix stiffness of 400-600 Pa, which is comparable to that of a normal liver, induced preservation of hepatocyte function, while a matrix with a stiffness of 1.2k to 1.6k, resembling that of a fibrotic liver, inhibited those functions [93]. Regarding porosity, a scaffold with 83% porosity seems to be optimal for hepatocyte culture, with average pore size ranging from 40nm to 70nm, shown by an increase in the synthesis of urea and the secretion of albumin by cultured hepatocytes [94]. These inherent, environment-independent mechanical properties are partially dictated by the materials used in the hydrogel. *In vivo*, mechanical properties are set by the proteoglycans and fibrous proteins that constitute the liver ECM. When attempting to replicate liver ECM *in vitro*, one can most easily influence the mechanical properties of the gel by the type and the density of the crosslinks between hydrogel molecules, be it through micropatterning, concentration of the hydrogel monomers, polymer length and polymerization temperature. Simultaneously, since native ECM exhibits an ever-changing dynamic behaviour, it is important that the properties of the hydrogel can be adapted or reversible [84].

Hydrogels for liver tissue engineering can be natural or synthetic, depending on whether or not they originate from organisms. Natural hydrogels are typically useful in cell culture, drug delivery and tissue engineering, but have the drawback that their properties can only be refined to a certain extent, besides their high complexity and their often xenogeneic nature [84]. Synthetic hydrogels, on the other hand, circumvent most of these problems by being completely engineered in a laboratory. However, their simplicity might make it harder to recreate the intricate environment of the liver extracellular matrix [84].

Natural hydrogels are particularly noteworthy in the context of this work, namely Matrigel® and fibrin hydrogels. While the former is a well-characterized xenogeneic matrix from mouse tumour, the latter does not have a fixed composition, since fibrin is the "backbone" of the hydrogel. Therefore, it is possible to include other components that affect the properties discussed above, such as liver ECM proteins, in order to provide the best environment possible for cell development [95]. Fibrin hydrogels are typically biocompatible and biodegradable, and the fibrin source can be autologous [84].

1.3.3 Microfluidics

Microfluidics deals with the manipulation of fluids in channels with dimensions up to tens of micrometers [96]. Having been developed recently, the appeal of microfluidics for biomedical applications lies in its ability to scale down biological processes, greatly decreasing the costs associated with studying them. By dealing in small volumes, it is possible to create integrated, sequential circuits in the same platform, performing multiple tests in a very short amount of time, even in smaller or lower-volume samples. This integrative platform is a so-called 'lab-on-a-chip' and is made up both of passive and active components that often allow for the mechanization of the testing process [97].

Naturally, the miniaturization of macroscopical phenomena is also a technical challenge that must be backed up the development of industry and appropriate production methods [97]. Owing to its three-dimensionality, high resolution and ability to be combined with other microfabrication technologies, two-photon polymerization is presented as a promising candidate regarding the manufacturing of lab-on-a-chip devices. However, other technologies, such as soft lithography, are also available, and are often used in the medical research field [98].

The basic principles of microfluidics are rather simple: scale down macroscopical phenomena to obtain a controlled environment. This causes a skew in the equilibrium between surface forces, which go from negligible at a macroscopical scale to crucial in a microfluidic setting, and volume forces, in which the trend is reversed [97]. Indeed, this can be seen in that fluids in microfluidic devices do not mix like smoke in the air. Furthermore, since viscosity has a dominant role over inertia, fluids in microfluidic channels typically experience laminar flow, which can be exploited or overcome, depending on the desired application [97]. Dimensionless parameter like Reynolds, Péclet or capillary numbers are particularly useful to help evaluate the equilibrium between inertia and viscosity, convection and diffusion and viscosity and surface tension, respectively. The higher relevance of surface forces when compared to a macroscopical scenario makes microfluidic devices particularly relevant in the study of barrier-like phenomena [97].

Fabrication of microfluidic devices through soft lithography will be of particular relevance for this work. As lithography characterizes the imprinting of a pattern onto a hard surface, soft lithography techniques deal with the fabrication of a structure by printing, molding, or embossing with an elastomeric stamp [99]. In the case of molding, which is useful for the manufacturing of microfluidic devices, it is common that an elastomer, such as polydimethylsiloxane (PDMS), is deposited onto a silica mask or wafer that has been previously made, by photolitography, for example. The elastomer is then processed by means of curing agents and temperature changes, forming a solid, yet flexible structure with the patterns of the silica

wafer [100]. This structure, upon retrieval from the the mold, can be used for microfluidic applications, depending on the size of the initial pattern. Currently, it is possible to produce structures with dimensions below 100 nm (so-called 'nanoprinting') by soft lithography [99].

1.4 Background and Objectives

Having seen how much promise organoids hold, when cultured in the appropriate conditions, and how much of a need for more advanced and accurate liver disease models than those currently available, one immediately starts to think about "the next step" in the development of even better models. Although the final goal of an intricate, perfect model of liver function might seem unattainable, small breakthroughs, when combined, might put us much closer to it than we initially thought. In fact, one could choose many different directions, like trying to build more complex organoids or systems, or to optimize external variables such as temperature and oxygen levels to perfectly match physiological values; however, there is one fundamental direction for which a proper solution has not yet been found in the culturing of organoids, spheroids and 3-dimensional structures in general: the vascularization of those structures.

The pressing need of adequately vascularized organoids arises when necrotic cores, structures full of dead cells that cannot receive nutrients and oxygen, are often recognized in three-dimensional cell aggregates [101]. Vascularization of organoids would allow for homogeneous distribution of nutrients and gases, as well as more efficient extraction of potentially toxic metabolites, which are currently done via diffusion [101] - a task that becomes increasingly difficult the further we go towards the center of the organoid. Vascularization could be leveraged even further in a setting where not only microvasculature would be created, but it would also be connected to larger vessels from an allogeneic subject, simulating human physiological bloodstream. These larger vessels would in turn be connected to nutrient reservoirs, be it in the form of medium reservoirs in *in vitro* culture or the blood stream of the host, in an eventual *in vivo* setting. Talking about the translation of this technology to an *in vivo* setting as a future application of such a system is not at absurd at all, since these "main" vessels to which the microvascular network is connected would allow for the transplantation of the whole system into a living host via microsurgery, which does not happen in most other forms of vascularization of 3D structures.

Furthermore, it is important to provide adequate support to the organoid, which simultaneously ensures sturdiness of the system, as well as providing tridimensionality and specific signaling cues to the cells. *In vivo*, as previously mentioned, this role is performed by the extracellular matrix. The extracellular matrix greatly influences the behaviour of cells/cell aggregates, through its mechanical properties (most notably stiffness and porosity) and through its chemical properties, via interaction of ECM proteins with the cells [84]. *In vitro*, the ECM can be emulated with an appropriate hydrogel. For this purpose, our group has previously developed a hydrogel based off a decellularized porcine liver extracellular matrix. The replacement of the traditionally used Matrigel with a liver ECM hydrogel is expected to yield better results for liver organoids, due to its organ specificity, and also opens the door for future human liver ECM-based hydrogels.

Lastly, fine control of culture conditions is required to achieve a relevant degree of vascularization.

One way to achieve such control is through the use of microfluidics - by placing the culture system inside a microfluidic platform, it is possible to greatly increase the control over medium flow and nutrient supply to the culture. For this effect, one other group member had developed a silicone-based (PDMS) microfluidic chip that allows for the encapsulation of cellular structures embedded in a hydrogel, while providing said structures with nutrients and medium.

Chapter 2

Materials and Methods

The present chapter deals with describing the methods employed in each procedure in a protocol-like fashion. Here, the methodologies are presented in chronological order of their use. Laboratorial work of this Master's thesis was done in the laboratories of Prof. Pedro Baptista (Instituto de Investigación Sanitaria de Aragón, Zaragoza, Spain) and Prof. José Manuel García Aznar (Instituto universitario de Investigación en Ingenería de Aragón, Zaragoza, Spain).

2.1 Cell culture

Cells were cultured in varying conditions, depending on the cell type, and following parameter established by previous experiences in the laboratory, as well as recommendations from the American Type Culture Collection [102].

HepG2 cells were cultured at 37°C in normoxia on a collagen type I (Col I)-coated dish of varying size, depending of the amount of cells and the desired application. The collagen coating was achieved by pipetting an adequate amount of collagen onto the dish so that the bottom surface was fully covered, letting it incubate for at least one hour at room temperature and removing the excess of ColI before seeding the cells onto the dish. The culture medium used was DMEM-based, with the addition of fetal bovine serum (FBS) at 5% concentration, as well as penicillin/streptomycin (P/S) at 1% and L-glutamine at 1%.

Human Umbilical Vein Endothelial Cells (hUVECs) were cultured at 37°C in hypoxia on gelatin-coated dishes of varying sizes, depending on cells number and experimental needs. The gelatin coating was applied by fully covering the culture surface of the dish with gelatin solution (0.2%), followed by an incubation of at least 30 minutes and the subsequential removal of the gelatin solution before cell seeding. hUVEC culture medium was MCDB 131-based, with 2% GlutaMAX™(GLX), 1% P/S, 2% FBS, insulin ($5\,\mu g\,mL^{-1}$) and transferrin ($10\,\mu g\,mL^{-1}$), as well as the vascular endothelial growth factor (VEGF) at $50\,ng\,mL^{-1}$, epidermal growth factor (EGF), fibroblast growth factor (FGF) and insulin-like growth factor 1 (IGF-1), all at $20\,ng\,mL^{-1}$. Alternatively, hUVECs were cultured in commercially available EGM-2 medium by Clonetics complemented with 1% P/S and 1% L-glutamine.

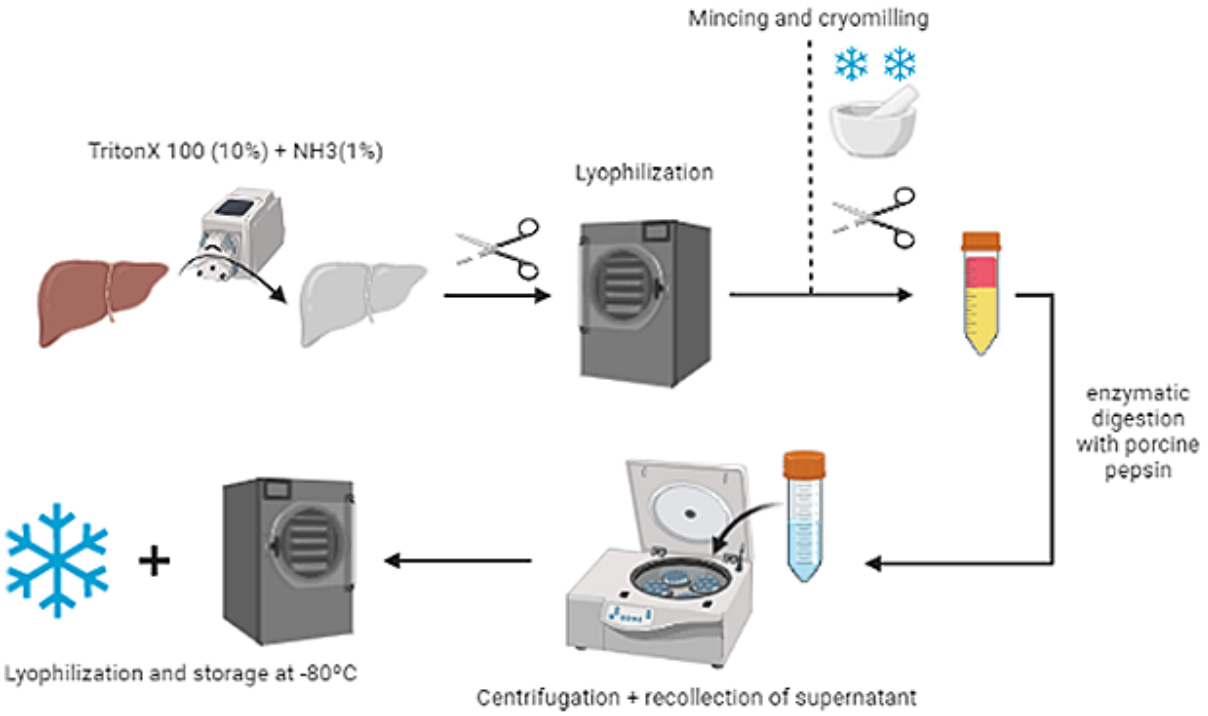

Figure 2.1: Overview of liver ECM processing workflow. After liver decellularization, adequate samples are sectioned and lyophilized Lyophilization results are then mechanically processed by mincing and cryomilling before undergoing enzymatic digestion cycles with porcine pepsin. Supernatants are collected and centrifuged, after which they are once more lyophilized. Created with BioRender.com.

Human Mesenchymal Stromal Cells (hMSCs or MSCs) were cultured at 37°C in hypoxia on gelatin-coated dishes of varying sizes, depending on cells number and experimental needs. The gelatin coating was performed as for hUVEC culture dishes. MSC culture medium is based off of DMEM/F12 and is supplemented with MSC-suited FBS at 10%, P/S at 1% and 1% L-glutamine in the case that the DMEM/F12 medium is not yet supplemented with GlutaMAX™.

Cell passaging was performed via trypsinization when 90-100% confluency was achieved, for HepG2 or hUVEC cultures, and whenever cell-to-cell contact was apparent in hMSC cultures, or whenever it was necessary for experimental reasons, with the aid of a trypsin-based solution. Cells were frozen in their native medium and dymethylsulfoxide (DMSO) in a cryocooler, initially at -80°C (overnight) and stored in liquid nitrogen the following day. Cells were counted in a Neubauer chamber by being resuspended in a solution with Trypan Blue contrast dye.

2.2 dECM-based hydrogel preparation

Figure 2.1 provides an overview of the preparation and processing of liver extracellular matrix, which is later incorporated in the fibrin hydrogel. The following subsections will concern themselves with thoroughly explaining each step of the method.

2.2.1 Liver decellularization

For the decellularization of the liver, the organ needs to be previously extracted from the subject via a partial or total hepatectomy, which will normally yield either one or both liver lobes, respectively. If possible, the surgery should be performed so as to preserve to vascular structure of the liver as well as the capsule of the organ, leaving a minimum of open ends or vessels.

Once extracted via partial hepatectomy, the right liver lobe of an adult pig liver was frozen at -30°C for 24h and thawed out at -4°C, in ice, for 2 days. It was weighted and a portion of the liver was taken for DNA analysis. The gallbladder was removed and liver was dried off with filter paper and sealed with superglue (cyanoacrylate) where its capsule had been damaged. At the site of the incision that separated liver lobules, which was more heavily damaged, gauze and cotton swabs were used to help stop the leaking. Four major vessels were left unsealed, chosen so that they could irrigate the entire liver when perfused. Plastic fittings were inserted into these vessels and fixated with superglue, simulating cannulation.

The decellularization process was carried out in 3 steps. Initially, the liver was suspended in a recipient filled with distilled water (dH_2O) and each of the four cannulated vessels was perfused with distilled water at a rate of 35 mL min^{-1} for 30 minutes, for a total of 4.2 L. Thereafter, a detergent solution consisting of TritonX-100 (panReac AppliChen) at 10% and ammonia at 1% in dH_2O was perfused through the liver. Initially, the perfusion was performed at 4 x 35 mL min^{-1} for four hours, then at 4 x 40 mL min^{-1} for two and a half hours, at 4 x 50 mL min^{-1} for two hours and finally at 4 x 70 mL min^{-1} for two hours, equating to a total detergent volume of 115.2 L. For the last step, the liver was washed via perfusion with dH_2O for at least twice the volume of detergent used, initially at 4 x 70 mL min^{-1} for 6 hours, then at 4 x 120 mL min^{-1} for a 4.5 hours, yielding a decellularized extracellular matrix (dECM). Flow was steadily increased and regulated in order to keep the liver at an adequate stiffness, at which it had some rigidity but the tissue was not under heavy stress, so as to preserve the vasculature and avoid leeks. The dECM was stored at 4°C with 3 drops of bleach for to enhance preservation and avoid contamination.

This decellularization protocol, although heavily based on previously existing liver decellularization protocols, was adapted in accordance with empirical observations due to the high variability in organ structure.

Characterization of liver decellularization by DNA quantification

Segments of decellularized porcine liver samples (first-grade and second-grade), as well as a segment of non-decellularized native pig liver, were collected and stored at -80°until the characterization of the decellularization.

DNA extraction was performed with the MasterPure™Complete DNA & RNA purification Kit (Lucigen). Initially, samples were weighted, mechanically disrupted, and mixed into 300 µL of Tissue and Cell lysis solution supplemented with 1 µL of Proteinase K. After an incubation at 65°C for 15 minutes, followed by a 5-minute incubation in ice, 150 µL of MPC Protein Precipitation Reagent was added to the 300 µL of lysed sample, with the resulting suspension being vigorously vortexed for 20s. Samples were pelleted by centrifugation at 4°C for 10 minutes at 13000 x g, after which each supernatant was collected

and transferred to 500 µL of isopropanol. Samples were then mixed by inversion for 30-40 times and centrifuged at 4°C for 10 minutes at 13000 x g. Isopropanol was then removed from the tubes, without touching the pellets, and each tube was thoroughly resuspended in 1 µL of 5 µg µL^{-1} RNAse A and 200 µL of Tissue and Cell lysis solution. The resulting mixture was incubated at 37°C for 30 minutes. Next, 200 µL of MPC Protein Precipitation Reagent were added to each of the 3 tubes, which were then vortexed for 10 seconds and placed in ice for 5 minutes. They were then once again pelleted by centrifugation at 4°C for 10 minutes at 13000 x g, after which each supernatant was collected and transferred to 500 µL of isopropanol. Samples were then mixed by inversion for 30-40 times and centrifuged at 4°C for 10 minutes at 13000 x g. Each sample was then rinsed twice with ethanol 70%, with particular care to not dislodge the pellet - if the pellet was dislodged, the sample was centrifugated again. Finally, ethanol was removed and sample DNA was suspended in 20 µL of TE Buffer.

DNA quantification was performed by NanoDrop spectrophotometry. For this, a calibration sample was used to set the baseline absorbance of TE Buffer, after which the absorbance of each sample at 260 nm, 280 nm and 230 nm was measured by pipetting 1 µL of it into the head of the NanoDrop device. The device head was cleaned in between uses.

2.2.2 Lyophilization, cryomilling, and digestion of decellularized matrix

Lyophilization and cryomilling of decellularized extracellular matrix

For the lyophilization of the dECM, the matrix was initially cut into smaller pieces, which were contained in distilled water in a urine cup in order to achieve the highest possible surface area/solution volume ratio, and frozen at -80°C. If preservation of cellular integrity is necessary, it should be frozen with liquid nitrogen so that cell walls are less prone to disruption by crystal formation. Transport to the lyophilizer was done in dry ice. The lyophilization of the dECM was performed via a Telstar lyophilizer located at the Instituto de Nanociencia de Aragón (INA) in Zaragoza, where the samples were left overnight to be lyophilized at 0.100mBar.

Lyophilized dECM samples were then cryomilled, by being cut into small pieces with surgical scissors and broken down into a fine powder via the conjugation of continuous deep-freezing with liquid nitrogen and mechanical work with mortar and pestle.

Enzymatic digestion of cryomilled dECM

Cryomilled dECM was digested at 20 mg mL^{-1} in a dH_2O solution with porcine pepsin at 1 mg mL^{-1} and 0.01M HCl for 48h at 37°C, with an agitation of 1200 rpm. Total solution volume was determined by the amount of dECM. Digestion products were then centrifuged at 4°C at 10000G for 10 minutes and the supernatant was collected and frozen at -30°C until matrix characterization. The pellet underwent a second, identical digestion and its supernatant was also collected and frozen. Characterization of the proteins present in the digested dECM was done by lyophilizing the matrix as previously described and performing a bicinchoninic acid assay (BCA) test (Thermo Scientific's Pierce™BCA Protein Assay Kit), whose protocol was thoroughly followed. In short, several sequential dilutions containing dECM protein

were made and then compared to standard solutions via absorption at 562 nm wavelength to obtain the total protein concentration of the processed dECM. Characterized matrix was then lyophilized in a urine collection cup and kept as a powder until used. The calibration line was calculated through the linear regression function of Microsoft Excel.

2.2.3 Production of dECM-based fibrinogen hydrogel

dECM-based fibrinogen hydrogels were made by mixing 3 base solutions (dECM solution, thrombin solution and fibrinogen solution) in equal proportions. These solutions have their unique composition, as listed below:

- dECM solution (in sterile H2O Milli-Q®):
  - hyaluronic acid (HA) at 6 mg mL^{-1};
  - dECM powder at 6 mg mL^{-1} (note: the concentration must be corrected according to BCA results);
  - MEM10X at 20%;
- fibrinogen solution (in sterile H2O Milli-Q®):
  - fibrinogen at 17.25 mg mL^{-1} ;
- thrombin solution (in sterile H2O Milli-Q®):
  - calcium chloride (CaCl2) at 120мм;
  - tranexamic acid (TXA) at 480 µg mL^{-1} ;
  - thrombin at 6.6 UmL^{-1};
  - MEM10X at 10%.

For the making of the hydrogel itself, the three solutions were initially prepared separate from each other in 3 different 1.5ml Eppendorf tubes, or similar. Working concentrations for each solution were three times as high as their concentration in the final hydrogel. The required amount of each reagent is determined by the necessary volume for each solution, which in turn depends on the desired amount of hydrogel.

Thrombin and dECM solutions were each mixed in their own tube and kept in ice. They were pH-corrected to basal medium values (indicated by a light pink colour) with NaOH and HCl solutions, and mixed together. The fibrinogen solution was made at room temperature and kept at 37°C to avoid precipitation, and swiftly mixed with the combination of dECM- and thrombin solutions via up-and-down pipetting only before applying the hydrogel onto the desired surface. In the case that there are multiple surfaces to be coated with the hydrogel, the tube with the hydrogel solution must remain in ice throughout the charging process. The hydrogel was left to polymerize for 1 hour at 37°C.

	1	2	3	4	5	6
A	dH2O	dH2O	dH2O	dH2O	dH2O	dH2O
B	dH2O	C1	C1	dH2O	Control	dH2O
C	dH2O	C2	C2	dH2O	Control	dH2O
D	dH2O	dH2O	dH2O	dH2O	dH2O	dH2O

Figure 2.2: Plate design for static co-culture of HepG2, hUVECs and hMSCs.

2.3 Static 3D co-culture of HepG2, hUVECs and hMSCs

2.3.1 Thrombin concentration experiment

This experiment consisted of the preparation of multiple hydrogel drops, each with a different thrombin concentration. This was achieved by modifying the thrombin concentration seen in section 2.2.3, and adjusting with increases or decreases in the volume of H_2O to keep the total volume of thrombin solutions at one third of the hydrogel volume, while keeping the rest of the composition of the hydrogel. Thrombin concentrations ranging from 2.1 UmL^{-1} to 2.5 UmL^{-1} were tested, with step-wise increases of 0.25 UmL^{-1}, for a total of 17 concentrations, prepared for a volume of 50 µL of hydrogel. Fibrinogen and dECM master solutions were prepared, with enough volume to account for 20 hydrogel drops when mixed. Each thrombin solution (volume = 13.33 µL) was then mixed with 13.33 µL of dECM solution and 13.33 µL of fibrinogen solution, resulting in a 50 µL hydrogel that was immediately pipetted onto a well of a 24-well plate as a drop.

Drops were incubated at 37°C for 1 hour, before sterile phosphate buffer saline (PBS) -/- was added to each drop-containing well and dH_2O was added to each other well, simulating static culturing conditions of cells in the hydrogel.

2.3.2 Experimental design

For this experiment, 2 conditions were considered, as well as one control, in which cell quantity and proportions varied according to table 2.1. Conditions, as well as the control, were duplicated.

Table 2.1: Experimental conditions for static co-culture of HepG2, hUVECs and hMSCs.

	Condition 1	Condition 2	Control 1
HepG2	12.500 cells	5.000 cells	No cells
hUVEC	10.000 cells	4.000 cells	8.000 cells
hMSC	2.500 cells	1.000 cells	2.000 cells
TOTAL	25.000 cells	10.000 cells	10.000 cells

The experiment was performed on a flat-bottom 24-well plate, with the plate design following the schematics shown in Figure 2.2.

Wells with dH20 were filled with 1mL of distilled water, whereas other wells contained one droplet of cell-laden hydrogel, and, after one hour of polymerization at 37°C, were filled with enough angiogenic medium to cover said droplet. These had been previously prepared in ways described the in following sections. Medium was changed when deemed necessary, or at least once every 3 days.

2.3.3 Angiogenic medium preparation

Medium was prepared according to the formulation seen in Table 2.2. Volumes were added from larger to smaller. Since pipetting volumes were extremely low for EGF, FGF and IGF-1, 3 uL of each of these factors were previously diluted in a 1:10 solution (in 0.1% bovine serum albumin (BSA), Tris 5mM + 0.1% BSA and 0.1% BSA, respectively) and a total of 6uL of each of the resulting dilutions was added to the medium instead. VEGF, EGF, FGF and IGF-1 were thawed out at room temperature, while all other materials had been refrigerated. The medium was filtrated with a syringe filter.

Table 2.2: Formula for the preparation of 30mL of angiogenic medium.

Medium component	*Volume*
DMEM F12	13.937mL
MCDB 131	13.937mL
L-glut (1%)	300uL
PS (1%)	300uL
FBS (5%)	1.5mL
Insulin (10mg/mL → 50ng/mL)	15uL
Transferrin (50mg/mL → 10ug/uL)	6uL
VEGF (1mg/mL → 50 ng/mL)	1.5 uL
EGF (1mg/mL → 20 ng/mL)	0.6uL (actually1.2uL)
FGF (1mg/mL → 20 ng/mL)	0.6uL (actually1.2uL)
IGF-1 (1mg/mL → 20 ng/mL)	0.6uL (actually1.2uL)

2.3.4 Cell preparation

Cells for the static culture experiment (HepG2 - pass 116, hUVEC - pass 4 and hMSC - pass 5) were thawed out as discussed in section 2.1 and cultured for 2 days, after which they were harvested and resuspended in the angiogenic medium referred to in section 2.3.3. Next, the cells were distributed in different Eppendorfs so as to allow for the different experimental conditions and centrifuged at 375g. The supernatant was aspirated, initially with a Pasteur pipette and later with a regular pipette tip, until a dry pellet was achieved.

2.3.5 Preparation of dECM-based fibrinogen hydrogel droplets

As discussed in subsection 2.3.3, the dECM-based fibrinogen hydrogel prepared for the static culture experiment was based off of 3 solutions. However, the total volume of hydrogel was 600µL and, therefore, the final formulation was derived by adapting the aforementioned concentrations to the desired final volume. Furthermore, the cells were incorporated into the hydrogel by scraping and up-and-down pipetting of the dry pellet mentioned in subsection 2.3.4 with the mixture of pH-corrected dECM and thrombin solutions in each tube, creating a homogeneous cell-in-hydrogel suspension. The tubes were put in ice

and the fibrinogen solution was then added to each individual Eppendorf tube and mixed via up-and-down pipetting.

Duplicates were made by taking two droplets of 50 µL each from each Eppendorf tube and placing them gently in a flat-bottom 24-well plate. The plate was incubated at 37°C for 1 hour to let the hydrogel polymerize.

2.4 Static 3D hepatic structures culturing

2.4.1 Tumouroid cultures

Tumouroids were cultured in a hanging drop. For that, HepG2 cells were initially cultured in 2 dimensions, as described in section 2.1, trypsinized and counted. Then, five cell suspensions of 100µL each were prepared so that HepG2 concentration in their culture medium (section 2.1) was, respectively, 1k per 30µL, 5k per 30µL, 10k per 30µL, 15k per 30µL, and 20k per 30µL. Three 30µL drops were made out of each cell suspension, which were placed on the inside of a lid of a 100cm^2 dish in 5 columns, according to cell concentration. The bottoms of the dishes were then then placed on the lids and the whole dish was flipped, leaving the cell-filled medium drops hanging. Cells were then incubated at 37°C until aggregates (tumouroids) were formed. This procedure was later upscaled to the point that each cell concentration had 15 drops (i.e. its own dish) instead of only 3 drops in a shared dish. Medium was not changed and tumoroids were frozen in their culture medium supplemented with 10%DMSO.

Later experiments used tumouroids made with concentrations of 5k, 10k, 15k and/or 20k HepG2 cells per drop.

2.4.2 Hepatic organoid cultures

The protocol for the formation of hepatic organoids was adapted from that utilized by the labs of Hans Clevers and Bart Spee and having suffered some modifications in our lab (Pedro Baptista).

Isolation of EpCAM+ cells

Initially, primary liver cells must be isolated from the liver. For this, samples were obtained from partial hepatectomies of donors with informed consent, processed by the Biobanco del Sistema de Salud de Aragón, and stored in DMEM high glucose (DMEM HG) medium supplemented with 1% P/S at 4°C. Prior to their dissosiation, samples from the liver tissue were taken for RNA extraction and for histology and stored in RNA preservation buffer (RNALater) at 4ºC, and in 4% paraformaldehyde (PFA) at room temperature, respectively. Fibrotic tissue, blood clots, scarred areas or remnants from surgical procedures were removed from the sample, which was then weighted.

Mechanical dissociation of the samples was performed by mincing the tissue submerged in DMEM HG supplemented with 1% P/S, 1% L-glutamine and 1% FBS with surgical scissors and forceps. Tissue and medium were then collected into appropriate-size tubes and washed to remove residual blood.

An enzymatic solution consisting of collagenase II (20.6mg per gram of tissue), DNAse I (10.3mg per gram of tissue) and Dispase II (12.3mg per gram of tissue) was prepared in 75mL of DMEM supplemented with 1% each of P/S, FBS and L-glutamine. If the sample weighted less than 2g, the enzymatic solution was prepared for a hypothetical weight of 2g, whereas, if the sample weighted over 3g, it was broken down and treated as two different samples. The sample was then placed in 15mL of enzymatic solution and incubated in a rotating orbital shaker at 37°C for 1 hour. Afterwards, the supernatant was collected, an additional 15mL of enzymatic solution were added to the sample and the suspension was incubated for 30 minutes. This last step was repeated as many times as necessary to get the highest possible amount of cells in suspension, although four repetitions per sample were usually sufficient. Simultaneously, the collected supernatants were centrifugated at 210 x g for 5 minutes at 4°C. The pellets were then resuspended in media containing 10% FBS, centrifugated again, and the resulting cells were resuspended in DMEM supplemented with 1% each P/S, FBS, and L-glutamine, and kept on ice until all the tissue digestions had finished. The supernatant of the initial digestion is centrifugated, its pellet is resuspended in FBS+10%DMSO, and frozen at -80°C, while supernatants from following enzymatic digestions were cultured on the day of the extraction to generate liver organoids.

Generation of organoids from adult stem cells

Remaining tubes, which contain organoid-forming human EpCam+ ductal cells, were resuspended together and centrifugated at 210 x g at 4°C, for 5 minutes. afterwards, they were resuspended in ammonium chloride red blood lysis cell buffer (8.3g/L NH_4Cl, 0.01M Tris-HCl adjusted to 7.5 ± 0.2 pH) and incubated at 37ºC for 10 minutes. Two washes with DMEM supplemented with 1% each of P/S, FBS, and L-glutamine were performed, followed by cell count in a Neubauer chamber, simultaneously assessing cell viability with the trypan blue exclusion method.

Cells were then resuspended in Matrigel® Growth Factor Reduced at 700.000 alive cells per 50 µL. Matrigel must be manipulated with frozen pipette tips and be kept in ice as much as possible until it gelates. The suspension of Matrigel and cells was then thoroughly mixed through up-and-down pipetting until cells appeared to be fully disaggregated from one another.

50 µL drops of Matrigel®+cell suspension were then plated one each into a well of a pre-warmed 24-well plate, which was then incubated at 37°C for 15 to 30 minutes, allowing for the gel to solidify. After gelation, 500 µL of human liver organoid culture medium were added to each well. Medium was changed every 2 to 3 days, and was freshly made every week.

Composition of liver organoid culture medium The culture medium for hepatic organoids is based off of Advanced DMEM-F12, being supplemented by a multitude of proteins, small molecules and growth factors. The full composition of the medium can be found in Table 2.3.

Table 2.3: Composition of hepatic organoid culture medium

Component	Concentration
Advanced DMEM/F-12	-----
L-glutamine	2mM
P/S	1x
HEPES	10mM
B27 (+ insulin/ - vitamin A)	1x
N2	1x
NIC 1M	10mM
ROCK inhibitor	10 µM
R-spondin	10% of total medium volume
NAC	1.25mM
A8301	5 µM
Forskolin	10 µM
FGF10	100 ng/ml
EGF	50 ng/ml
HGF	25 ng/ml
Gastrin	10 nM

Organoid passaging

Passages were performed every two weeks or if signs of degradation were apparent in Matrigel® drops. Initially, Matrigel®+organoid drops were mechanically scraped off of the culture well with the aid of a pipette tip and transferred to a 15 mL tube. The well was then washed with cold DMEM to harvest any remaining cells into the same 15 mL tube. Up-and-down pipetting was employed to dissolve Matrigel clumps, followed by a centrifugation at 210 x g for 5 minutes at 4°C.

The pellet, which contained organoids and Matrigel® , was then treated with TrypLE Select, with the resulting suspension being incubated in a 37°C bath for 15 minutes. The incubation step was repeated until no organoids were seen in suspension. Tubes were then centrifugated at 210 x g for 5 minutes at 4°C and the pellet (organoid-forming single cells) was resuspended into an appropriate volume of Matrigel® so as to achieve a density of 300.000 cells per 50 µL of Matrigel® . 50 µL drops of the suspension were then seeded in the appropriate number of wells of pre-heated 24-well plates and left 15 to 30 minutes to incubate, after which 500 µL of human liver organoid culture medium were added to each well.

Organoid and tumouroid harvestings

Harvesting of 3D structures, both organoids and tumouroids, followed a similar protocol, which differs only in the initial harvesting process. While tumouroids were simply aspirated with the help of a pipette tip and transferred into an Eppendorf tube which was centrifugated to create a tumouroid pellet, organoids, being embedded into Matrigel® , required a more delicate procedure. Thus, organoids were harvested by mechanical scraping of the Matrigel® drop after the removal of old culture medium and the addition of 1 mL of cold Advanced DMEM/F-12. The drop was transferred to a 15 mL tube and the well was washed with cold Advanced DMEM/F-12, which was then transferred to the same 15 mL tube to ensure that all cells had been collected. The suspension of gel and cells in Advanced DMEM/F-12 was mixed by

up-and-down pipetting until it appeared to be homogeneous and was then centrifugated at 210 x g for 5 minutes at 4°C. After the centrifugation, the supernatant is removed and the pellet is resuspended in more cold Advanced DMEM/F-12, until a volume of 5 mL is met. These steps were repeated until the Matrigel® can no longer be seen in the pellet.

2.4.3 mRNA characterization of tumouroids, organoids, hUVECs, HepG2 cells and native liver

mRNA characterization was obtained via reverse transcription polymerase chain reaction (RT-PCR) of lysed tumouroids and organoids. Initially, the structures were harvested as seen in subsection 2.4.2, but were directly placed in 100 µL or 300 µL TRIzol™reagent (depending on sample size). 2D-cultured hUVEC and HepG2 cells were harvested by trypsinization of the culture, neutralisation with FBS-supplemented medium and centrifugation. The pellet was then resuspended in TRIzol reagent. Cells and three-dimensional structures resuspended in TRIzol were stored at -30°C until they were needed for mRNA isolation.

For mRNA isolation, samples were thawed out and 0.2 mL of chloroform were added to each sample per every mL of TRIzol. Samples were vortexed, rested for 2-3 minutes and centrifuged at 4°C for 15 minutes at 12000 x g. The resulting transparent phase was transferred to another tube, to which 0.5 mL of isopropanol were added per mL of TRIzol. The resulting solution was vortexed and placed in ice for 10 minutes. The solution was then pelleted by centrifugation at 4°C for 10 minutes at 12000 x g, the supernatant was discarded, and the pellet was washed with 1 mL of 75% ethanol solution. Samples were then vortexed and centrifuged at 7500 x g for 5 minutes at 4 °C. Lastly, the supernatant was discarded and the pellet was resuspended in DEPC water. Results for RNA purity and quantity were measured by a NanoDrop microvolume spectrometer.

cDNA was created from the mRNA sample by adding reverse transcriptase and incubating for 10 minutes at 25 °C, 30 minutes at 42 °C, and 5 minutes at 85°C. Samples were then cooled at 4 °C before being prepared for polymerase chain reaction (PCR) assays.

Primers for human VEGF, HiF1-α, HGF, Ki-67, ITGB1, ITGB3, NOS3, ETV2, COX-2, KLF2 and RAP1 genes were determined with ncbi's primer designing tool [103]. Verified primers for GAPDH, albumin genes already existed in the lab. PCRs were then carried out in temperatures from 54°C to 64°C with a two-degree step increase to assess the optimal working temperatures of each primer, while simultaneously verifying the amplification of mRNA for each gene, for each sample.

Sample preparation for PCR essay was done by calculating the total number of conditions (primer and sample combinations) for each temperature, and adding 10 µL of DNA AmpliTools Green Master Mix and 8 µL of H_2O MilliQ to each 100 µL PCR tube. Tubes were then filled with the appropriate samples and primers, and incubated in a thermocycler. Primers for ITGB1, ITGB3, NOS3, ETV2, COX-2, KLF2 and RAP1 genes were tested with hUVEC samples, as well as liver samples, at 54°C, 56°C, 58°C, 60°C, 62°C, and 64°C. Additionally, tumouroid, organoid, HepG2, and liver samples were tested with Hif1-α, HGF and Ki-67 primers at all temperatures, as well as with VEGF primers at 58 °C and ALB primers at 64°C. All

samples were incubated with GAPDH primers at 58°C and 60°C. Incubation cycles were made up of 3 stages: initially, all samples were incubated at 95°C for 5 minutes. Then, 35 repeating incubation cycles were done, where the samples would initially be incubated at 95°C for 30 seconds, then at specified the temperatures (as seen above) for 30 seconds, and then at 72 °C for 45 seconds. Lastly, samples were incubated at 72°C for 5 minutes before being cooled to 4°C and frozen at -30°C until being classified by gel electrophoresis.

For the gel electrophoresis of PCR results, gels of 2% agarose dissolved in Tris-Borate-EDTA Buffer were made. Dissolution of agarose was ensured by microwaving the solution to the point of ebullition and mixing it by agitation. The gel solution as then placed into molds with 30-tooth combs, and left to cool at room temperature. Once the gel solidified, the combs were removed, and the gel was placed in an electrophoresis tub and covered with Tris-Borate-EDTA Buffer. Samples were then loaded into the gel in sequential order, as well as a ladder to track sample progression, and the gel was left to run at 100 V for 30 to 45 minutes, depending on visual cues. Gel visualization was done with Bio-Rad's Gel Doc™EZ Imager, as well as their proprietary software.

2.5 Dynamic cell culture in bioreactor

2.5.1 Bioreactor setup

The bioreactor consisted of circuits of silicone tubes connected to the microfluidic device which were driven by a Hei-FLOW Precision 01 peristaltic pump lent to us by José Manuel García Aznar's lab at the I3A. Each chip was connected to two circuits: artery (top) and vein (bottom). Silicon tubes by MaterFlex® (with an inner diameter of 1.4mm) were attached to each other with proper fittings and four-way stopcocks, which were used to purge the circuit from large, static air bubbles, to prime the circuit checking for leaks, and to change the circuit's medium. 20 mL syringes were used as medium reservoirs (one for each circuit), where the piston was set at roughly 10 mL, which were filled 50/50 with air and culture medium. These were connected to the circuit via their usual outlet, but through a hole drilled into the syringe's wall as well, since a circular circuit was needed.

2.5.2 Culture conditions

Cells were cultivated at 37°C, in normoxia, for different time frames and with different media, depending on the experiment. Whenever hUVECs and hMSCs were cultured, but not HepG2, the culture medium was the one used for hUVEC cultures, as mentioned in section 2.1. Whenever HepG2 cells or tumouroids were present alongside hUVECs and hMSCs, the culture medium mentioned in section 2.3.3 was used as bioreactor medium. Flow was set at 2mL min^{-1}, but was not always maintained throughout the entirety of the experiments, being turned off for as long as 48h when empirically deemed necessary, in order to cause a state of starvation in cultured cells. Partial or total medium changes occurred at most every 5 days, or whenever necessary due to medium usage or leak in the circuit.

2.5.3 Liver-free angiogenic assay

For this experiment, cells were prepared as described in subsection 2.3.4, with the difference that a total of 300k cells were prepared per microfluidic chip, of which 80% (240k) were hUVECs and 20% (60k) were hMSC. No HepG2 cells, tumouroids or organoids were included in this experiment. Upon preparation of the dry cell pellet, cells were suspended in 120 µL of hydrogel or 120 µL of Matrigel® which was always handled with cooled pipette tips. 60 µL of cells suspended in Matrigel went into the central chamber of chip 1 (with 15 µL being pipetted every time), while the central chamber of chip 2 was filled with the same amount of cells suspended in fibrinogen-based hydrogel. Custom dECM hydrogel was used for all following liver-free angiogenic assays. Lastly, a previously cut small, ring-like segment of blood vessel previously isolated from a blood vessel was inserted through the central port of each chip, as thoroughly described in the literature [104]. This process must be performed swiftly, to avoid untimely gel polymerization, yet carefully, to avoid air bubbles. The system was left to polymerize for 1 hour before it was incorporated into a bioreactor with angiogenic medium, as described in subsection 2.5.2.

The dynamic culture system was maintained for up to two weeks, and was imaged daily. Medium was changed whenever leaks caused the medium reservoirs to be depleted, or once every 4 days. An irregular system of days with and without medium flow was implemented, and the system was evaluated every day.

Having seen promising developments in some of the attempts made, the structures in those chips were fixed by perfusion with PFA 4% through both artery and vein perfusion channels for 15 minutes, after which they were stored at room temperature.

2.5.4 Tumouroid and Organoid angiogenic assays

For angiogenic essays with tumouroids or organoids, the protocol replicated the one followed in liver-free angiogenic essays, as presented in section 2.5.3. However, for the case of tumouroids, those of sizes ranging from 5k cells to 20k cells were introduced in the hydrogel and therefore in the microfluidic chip alongside hUVECs and hMSCs. Like hUVECs and hMSCs, tumouroids had been centrifugated into a dry pellet before being resuspended in the hydrogel. Different experiments were carried out to determine the best type and amount of tumouroids to introduce in the hydrogel, which are further detailed in Table 2.4.

Organoids used in dynamic culture assays were harvested and processed as described in section 2.4.2 up until the obtention of a pellet consisting only of organoids. This dry pellet was resuspended into the hydrogel alongside other cells, and introduced into the central chamber. For organoid-based angiogenic assays, a hybrid organoid and angiogenic medium was used, which is further detailed in Table 2.5. Additionally, all tumouroid- and organoid-related assays were performed with dECM-based fibrin hydrogel, and none with Matrigel® .

Table 2.4: Details of the experimental design of each tumouroid-based bioreactor setup, regarding the types of tumouroids used (determined by the amount of cells in each tumouroid), the relative proportion of each type, the amount of tumouroid structures and cells inserted in the culture system, the presence or absence of a ring-like blood vessel segment in the central chamber and total run time of the experiment. T1-T4 represent 4 different trials for tumouroid angiogenic assays.

	T1	**T2**	**T3**	**T4**
Tumouroid types (x 1000 cells/drop)	10, 15, and 20	10, 15, and 20	10	5
Relative proportion (%)	33 each	33 each	100	100
Amount of tumouroids in the device	5 + 5 + 5 = 15	5 +5 + 5 = 15	10	20
Amount of tumouroid cells (x 1000)	50+75+100 = 225	50+75+100 = 225	100	100
Total cells in device (x 1000)	525	525	400	400
Ring in central chamber	No	Yes	Yes	Yes
Run time (days)	13	9	13	12

2.5.5 Imaging

Day-to-day imaging

Day-to-day pictures of cell cultures, both in static and dynamic conditions, were obtained with NIS Elements 3.0 software in combination with the Nikon DS-Fi1 camera attached to the Nikon Eclipse TS100 microscope.

Fluorescence time-lapse imaging

For the fluorescence time-lapse imaging, the setting of of a bioreactor was emulated, in which medium perfused chips that had previously been fixed with a 4% PFA solution. For the purposes of fluorescence imaging, fluorescein isothiocyanate–dextran (FITC-Dextran) was dissolved into the medium at a concentration of 25 mg mL^{-1}, which was perfused at 0.6 mL per minute. The fluorescence time-lapse images, as well as high-resolution images, were obtained with a widefield time lapse Leica AF6000 microscope and recorded with the LAS X software at an exposure of 23 ms.

Table 2.5: Composition of hybrid angiogenic/organoid medium for dynamic angiogenic assays with liver organoids. GLX, P/S, EGF and FGF concentrations were omitted from one medium composition to avoid redundancy when the medium component was present in both the angiogenic and organoid-related aspects of the medium.

Angiogenic component		**Organoid component**	
MCDB 131	(50% of leftover volume)	Advanced DMEM/F12	(50% of leftover volume)
GLX	2%	GLX	---
P/S	---	P/S	1x
FBS	2%	HEPES	10mM
Insulin	5 µg/ml	B27 (+ins/-vit A)	1x
Transferrin	10 µg/ml	N2	1x
VEGF	50 ng/ml	NIC	10mM
EGF	---	ROCK inhibitor	10 µM
FGF	---	R-spondin 1	10%
IGF-1	20 ng/ml	NAC	1.25mM
		A8301	5 µM
		Forskolin	10 µM
		FGF10	100ng/ml
		EGF	50 ng/ml
		HGF	25 ng/ml
		Gastrin	10nM

Chapter 3

Results and Discussion

The present chapter deals with the presentation and discussion of the results obtained in this work. The discussion of results is structured in such a way that, in each experiment, the depth of the discussion increases in each successive paragraph. This incorporation of the discussion with the results accounts for a thorough examination of each experiment, without losing the overarching view of the impact of the research.

3.1 Manufacturing of dECM-based fibrin hydrogel

As can be seen in Figure 2.1, the production of a dECM hydrogel is a multi-step procedure, which will be explored in this section. Initially, a porcine liver is obtained and decellularized. Then, the decellularized extracellular matrix is mechanically and chemically processed to solubilize its proteins. These proteins are then characterized by a BCA Protein Assay, after which the hydrogel can finally be assembled.

3.1.1 Liver decellularization

Porcine liver was obtained through partial hepatectomy of the left liver lobule, appropriately cannulated and sealed, washed by perfusion with dH_2O, and decellularized by perfusion with a TritonX-100 and ammonia-based solution. Perfusion rates ranged from 35 $mL\,min^{-1}$ to 70 $mL\,min^{-1}$, so as to ensure rigidity of the perfused tissue, with the liver lobule being perfused for a total of over 10 hours by over 115 L of detergent solution. In this case, since the structure was not necessary to be used as a scaffold, structural integrity of the blood vessels was not a major concern, therefore allowing higher pressures that enabled thorough perfusion of the organ an its subsequent decellularization.

The porcine liver gradually turned white during the perfusion with TritonX-100, as can be seen in Figure 3.1 a) and b), becoming almost transparent in some border regions. Large as well as small vessels became increasingly apparent as the tissue was the decellularized, showing a vascular tree that appeared to be mostly conserved throughout the decellularization process. Decellularization results were evaluated by measuring the amount of DNA present in the samples as characterized by NanoDrop spectrophotometry, with collected samples ranging from over 97% decellularization to over 81% decellularization, as calculated

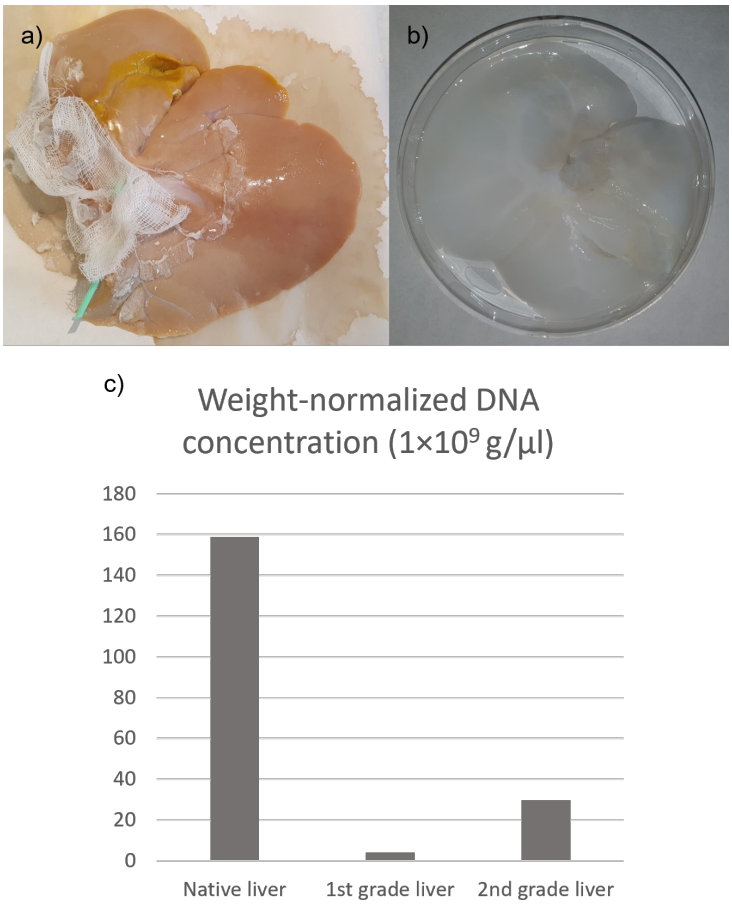

Figure 3.1: Decellularization of porcine liver. a) Non-decellularized, sealed porcine liver. b) Decellularized porcine liver. c) Efficacy of decellularization protocol. 1^{st} grade liver samples showed over 97% decellularization ratios when compared to native, non-decellularized liver, while over 81% decellularization was achieved for 2^{nd} grade liver samples.

by dividing weight-normalized concentration ratios between decellularized liver samples and native liver sample. Results can be seen in Table 3.1 and in Figure 3.1 c). A260/A280 and A260/A230 absorbance ratios also show that the samples are mostly pure and protein-free, and that the content of aromatic compounds such as TRIzol is slightly elevated when compared to literature [105, 106]. All in all, samples can be considered pure. So called 'first-' and 'second-grade' samples are a result from direct observation of decellularized tissue: some areas that presented typical signs of decellularization appeared to be completely clean, with no traces of any cells (these areas were typically found around the edges of the tissue), while other areas seemed to have been sufficiently decellularized for our purposes, but did not seem to be as clean or cell-free. Thus, to avoid waste, both sample types were collected, being distinguished by calling them '1^{st}-grade' and '2^{nd}-grade', respectively.

Steady perfusion with a soft detergent-based solution was an effective method for the decellularization of porcine liver. Indeed, as described by Baptista et al [107]. in the beginning of the last decade, decellularization of vascularized liver with a soft detergent not only allows for conservation of the vascular tree, but also yields better results than the previous method, which was a combination of mechanical and chemical decellularization [108]. The decellularization results seen here are on par with those observed in the literature. The future possibilities for improvements and applications of decellularization techniques,

although enticing, are outside the scope of this work.

Table 3.1: Decellularization results of adult porcine liver. Decellularization ratios of 97.74% and 81.31% were obtained for 1^{st}- and 2^{nd} grade liver samples, respectively, with DNA/protein purity levels of 1.9553 for 1^{st} grade samples and 1.9821 for 2^{nd} grade liver samples. Purity respective to organic compounds such as TRIzol reagent was measured by A260/A230 ratios.

	Native Liver	1^{st} grade decellularized liver	2^{nd} grade decellularized liver
Concentration (ng µL^{-1})	2385.2	74.4	493.2
Weight-normalized concentration (ng µL^{-1})	159.01	4.133	29.71
Decellularization ratio	NA	97.74%	81.31%
Absorbance at 260 nm (A260)	47.7	1.49	9.86
Absorbance at 280 nm (A280)	23.9	0.761	4.98
A260/A280	2.00	1.96	1.98
A260/A230	1.85	1.53	1.7

3.1.2 Liophilization, digestion, and cryomilling of decellularized liver ECM

The main goal of this step was the obtention of proteins that are typically characteristic of the extracellular matrix of the liver. In fact, pepsin digestion of decellularized extracellular matrix has been shown to solubilize dECM proteins, allowing for their integration into a hydrogel [109]. Mechanical steps incorporated in this method, such as lyophilization and cryomilling, serve the purpose of giving the collected dECM the adequate form (in terms of rigidity and size, respectively) for its further processing. The *de facto* results of the enzymatic digestions will only become apparent in the characterization of the quantity of protein in the supernatant.

3.1.3 BCA Assay

For the BCA assay ,a calibration function was calculated based on BSA absorption (Appendix 1) with a simple linear regression, having obtained a the equation y = 1,2961x + 0,0742 , with R^2 = 0,9962. Adequately substituting the concentration of our sample gave us a correlation factor of 0.3015, meaning that, for every gram of liver dECM powder, we have an expected 0.3015g of dECM proteins. Given that this is an intermediate step, it is not often discussed in the literature. Nevertheless, it is adequate to assume their validity, since a proteic yield of roughly 30% is perfectly reasonable. This yield could be enhanced by optimizing the protocol for matrix decellularization, as well as the protocol for enzymatic digestion.

3.1.4 Production of dECM-based fibrinogen hydrogel

The last step in the hydrogel manufacturing process is the combination of all 3 key elements of the dECM hydrogel: fibrinogen, thrombin and dECM. The role of the decellularized extracellular matrix is to allow for the hydrogel to emulate the environment of the liver, whereas fibrinogen and thrombin are responsible for the backbone of the hydrogel. Thrombin interacts with fibrinogen fibrinopeptides, cleaving the fibrinogen molecule into fibrin monomers that rapidly polymerize [110], thus encapsulating dECM proteins in a three-dimensional network. This creates an environment akin to that of the liver, facilitating cell-cell interactions, but also cell-matrix interactions. Working concentrations of each solution are three

times as high as their final concentration in the hydrogel to allow for adequate 1:3 mixing of each solution into the hydrogel.

We have found the hydrogel to be capable of forming cohesive, self-containing drops in which cells can proliferate, as well as apparently sound three-dimensional microfluidic structures. Polymerization was effective to the point of the hydrogel polymerizing in the pipette tip if not kept on ice, assuming adequate concentrations of each component and a neutral pH value, as indicated by a light pink colour. However, parallel experiments in our laboratory have found that, as with many growth factors, 'freezing-thawing' cycles of its components (namely thrombin) can severely hinder or even prevent hydrogel polymerization altogether, which will almost surely have negative effect on any cell-culturing assays performed on it.

3.2 Static 3D co-culture of HepG2, hUVECs and hMSCs

Before any biologically relevant experiment was conducted, a trial was carried out to determine the optimal thrombin concentration for hydrogel polymerization (Figure 3.2a). Going from a previous protocol, hydrogels were made with step-wise increases in thrombin concentration of 0.025 UmL^{-1}, ranging from 2.1 UmL^{-1} to 2.5 UmL^{-1}. Optimal thrombin concentration was found to be 2.2 UmL^{-1}, with this result being applied in all hydrogel cultures of this work.

Upon optimization of the hydrogel, a static co-culture experiment with hUVECs, hMSCs and HepG2 cells in 50mL hydrogel drops (Figure 3.2 was conducted to provide a proof of concept for the comparison of culturing in static versus dynamic conditions. In static conditions, medium change occurred when deemed necessary, or at least once every 3 days.

This experiment had two parallel goals: on one hand, it served as a tryout for *in vitro*-generated angiogenesis; on the other, the difference between experimental conditions and control allows us to infer on the influence that HepG2 cells have on neovascularization. Given their tumorigenic phenotype, HepG2 cells were expected to secrete angiogenic factors that would aid in the organization of hUVECs into small blood vessels, with the latter possibly exhibiting trophotropic behaviour in relation to the former.

Thus, hUVECs, hMSCs and HepG2 cells were cultured in liver dECM fibrinogen-based hydrogel drops as described in subsection 2.3.2, with results shown in Figure 3.2 c) and d). Upon seeding, cells seemed homogeneously distributed throughout the drop, with very few clumps or aggregates. The drops polymerized in a cohesive manner, without apparent cracks or flaws. Organization of some type can be seen after four days of culture, but not in a degree that grants it any significance for the purposes of this experiment, nor in any typical form for the formation of new blood vessels. Furthermore, hydrogel drops degraded over time, which caused the cells to latch on to the bottom of the plate, defeating the purpose of a 3D culture. The degradation of hydrogel drops was also one of the reasons for an early stop to the experiment, since it became impossible to maintain a reliable 3D culture without having to passage the cells and seed them onto a different plate in a new hydrogel drop. These results were seen in all drops, for all conditions, with very little variance.

At a first glance, one might initially conclude that static 3D culture does not foster the adequate environment for neovascularization of HepG2 cells, nor for the self-organization of hMSC-supported

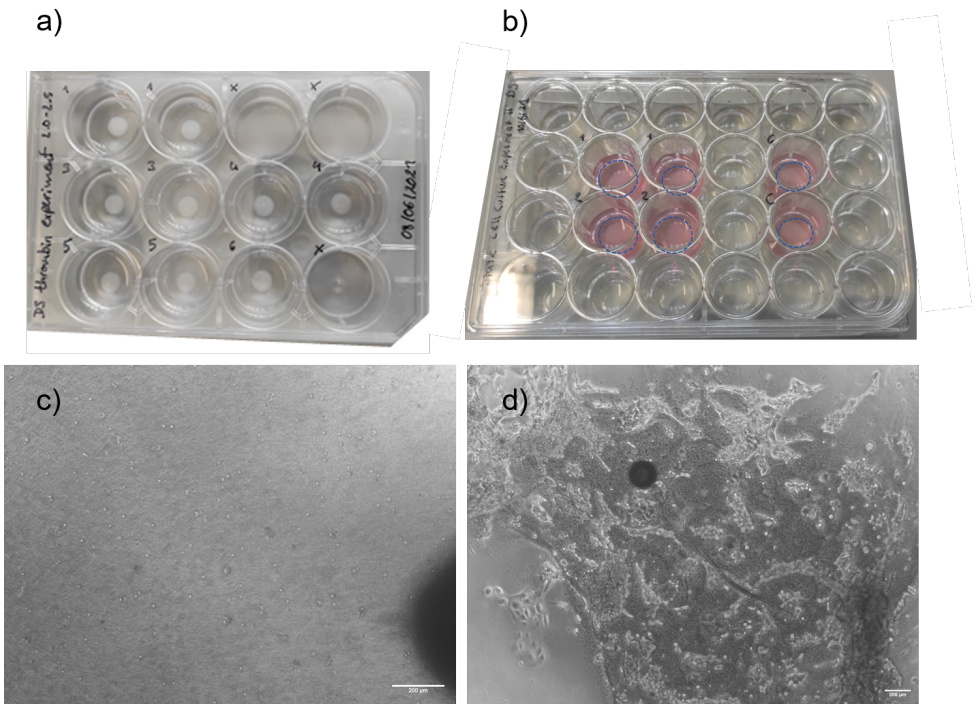

Figure 3.2: a) Plated hydrogel drops to determine thrombin concentration for best stiffness. b) Macroscopic image of three-dimensional static co-culturing of hMSCs, hUVECs and HepG2 in a fibrin hydrogel. c) Microscopy imaging (4x amplification) of culture condition 1 (well B2) at culture day 0. d) Microscopy imaging (4x amplification) of culture condition 1 (well B2) at culture day 5. Scale bars = 200µm.

hUVEC into blood vessel-like structures. However, there are multiple accounts of extensive, reputable research that proves the opposite, meaning that our results must be carefully examined.

Despite having results that support our approach that dynamic culturing favours angiogenesis through mechanical stimulation, critical thinking shows various shortcomings of the experiment. For one, it was repeated an insufficient amount of times, with each condition only being assigned 2 wells. Duplicates, despite being more robust than singlets, are still flawed and prone to high variability. However, since the results were propagated throughout all conditions, it is is prudent to look at other possible sources of error. There was also visible degradation of the hydrogel drops throughout the experiment, as they disaggregated in patches, which was most likely due to medium changes being performed too abruptly. Ultimately, this led to cells attaching to the plate surface, turning a 3D culture into a 2D one, which can heavily impact cell migration and cell-cell and cell-matrix interactions. Most importantly, however, the amount of cells suspended in each drop, as well as their proportions, might have just been wrong. Although an educated guess led to the inclusion of HepG2 cells, hUVECs and hMSCs in 50/40/10 proportion, respectively, there was no confirmation that those proportions were suited for co-culture of these cell types with the goal of *de novo* angiogenesis. Similarly, there was no confirmation that the amount of cells used in each condition was appropriate to stimulate angiogenesis in a 50 µL drop.

However, it is important to keep in mind that this experiment was mostly just a proof of concept for static culturing, even more so due to the absence of an adequate dynamic culture comparison with all three cell types. Even for the case of co-culture of hUVECs and hMSCs, the culturing time was far superior in

dynamic cultures. Therefore, the results of this experiment are not necessarily invalid, since they provide a good starting point for the development of experimental designs that can be used in dynamic culture systems.

3.3 Static 3D hepatic structures culturing

3.3.1 Static culture for HepG2 tumouroid assembly

HepG2 spheroids (also called 'tumouroids') were cultured via hanging drop method. In short, the desired number of cells was suspended in 30 mL drops on the inside of the cover of a Petri dish. Upon being turned upside-down, the drops were acted upon by the force of gravity, pulling them down, but also by surface tension, which kept the drops connected to the plate. However, since surface tension does not apply to the inside of the drop, cells naturally aggregate near the low point of the drop. Due to cell-cell interactions, and the tendency to adhere to other surfaces, cells bind to each other, forming a three-dimensional aggregate. Thus, each drop resulted in one HepG2 spheroid - a tumouroid.

Different concentrations of cells per drop were tried, in order to optimize the result for microfluidic applications. An initial trial with drops containing 1k, 5k, 10k, 15k, and 20k cells each was performed to observe the behaviour of the cells and structures in those culture conditions. It was found that the hanging drop method was effective in forming 3D HepG2 aggregates at all concentrations after only 5 days of hanging-drop culture. Figures 3.3 a) to d) show the results of static tumouroid assembly cultures, although the results for 1k cell-drops were not included, due to their irrelevance for future experiments. Tumouroid size increased significantly when comparing drops with 1k and 5k cells, and further when comparing 5k cell-drops with 10k cell-drops. However, increasing cell concentration from 10k per drop to 15k or even 20k does not represent a significant increase in tumouroid size, if at all any.

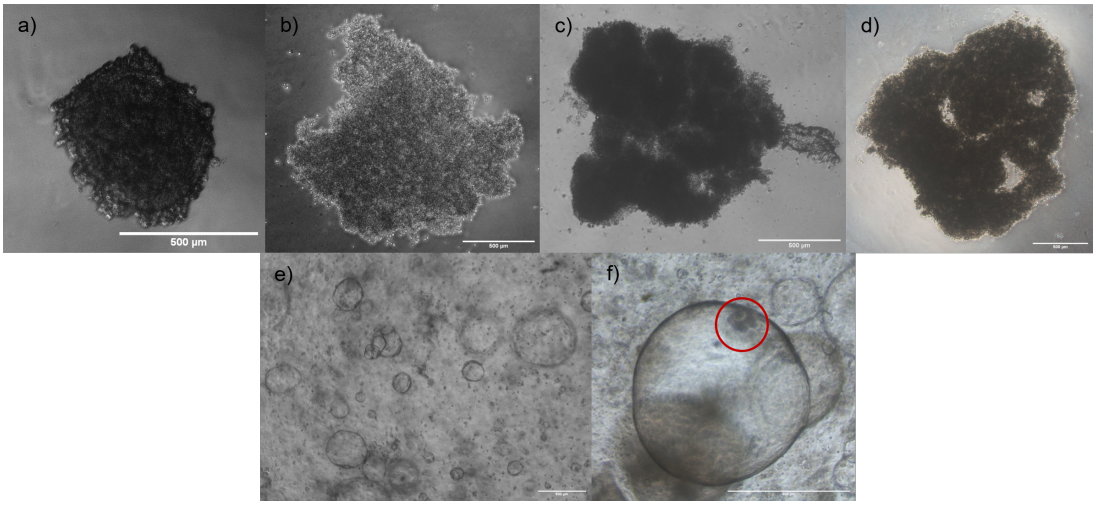

Figure 3.3: a)-d) Static, three-dimensional culture of HepG2-based liver tumouroids with 5k, 10k, 15k and 20k cells per 30 ul drop, respectively. Structures seem cohesive, with size discrepancies between 5k cell-structures and bigger tumouroids. e) Static, three-dimensional culture of hepatic organoids (4x). f) Close-up on static organoid culture, highlighting an internal structure of the organoid (10x). Scale bars = 500 µm

In fact, there seems to be a limit to the size of 3D HepG2 aggregates, causing higher density of cells instead of larger volume. A possible explanation is that this phenomenon might be an adaptation to try and minimize necrotic cores, which have been seen to be dependant on the size of the aggregate [111], since surface-to-volume ratio grows according to the square-cube law, and diffusion is a surface-based process. In fact, while the surface area of the sphere is determined by $A = 4\pi r^2$, where A is the surface area of the spheroid and r is its radius, the volume of the spheroid can be roughly calculated with the formula for the volume of a sphere, namely $V = \pi r^3 \times 4/3$, where V is the volume of the aggregate and r is its radius. This means that the ratio of volume-to-surface area is given by $V/A = r \times 1/3$. Its direct dependence on the radius implies that, the larger the spheroid grows, the more accentuated the discrepancies between surface phenomena (such as diffusion of gases and nutrients) and volume phenomena become. By reducing the increase in sphere radii, opting for condensation instead of expansion, the ratio of Volume/Surface Area is not as heavily affected, meaning that the transport of nutrients and gases, which have to travel the entire distance of the spheroid's radius to reach its core, is not as heavily hampered.

3.3.2 Static culture for hepatic organoid generation and propagation

Hepatic organoids were formed by isolation, processing and conditioning of EpCAM-positive ductal cells from native human liver. In the isolation process, the liver tissue was processed both mechanically and enzymatically. Ductal cells were then plated in Matrigel® drops on a 24-well plate and conditioned to self-assembly into organoids in an appropriate medium supplemented with r-spondin, A8301, and other necessary growth factors. Organoids were passaged every two weeks, or whenever Matrigel® drops seemed to degrade.

This section of the work was performed with assistance of more experienced colleagues, due to the precise nature of the organoid formation protocol.

The isolation of EpCam-positive cells and the subsequent generation of hepatic organoids were successful, resulting in semi-transparent, self-enclosed structures with the expected morphology. Unlike what happened with tumouroids, each drop contained multiple organoids of varying sizes (Figure 3.3 e)). Furthermore, as can be seen in Figure 3.3 f), organoids contained secondary structures inside them. Being self-enclosed, organoids in a drop can be considered separate entities independent from one another, each with the capacity to simulate liver behaviour. Taking advantage of the small size of the organoids, it is therefore possible to obtain a statistically significant representation of the liver by eliminating the variance associated with each organoid structure if multiple organoids are subject to the same culture conditions and stimuli. This principle, which can also be applied to tumouroids, is the motivation behind high-throughput screening, a testing philosophy that shows great promise for drug screening and for the study of responses of the organ to external stimuli [112].

Interestingly, organoids, unlike tumouroids, do not appear to show a size limit for each individual structure. This can be explained by the fact that they are self-enclosed and mostly hollow, meaning that, even at a high volume, their cell density would still be low enough not to impact in diffusion phenomena. However, the most plausible explanation is that the organoids simply have not yet reached the size of the

Table 3.2: Results of mRNA extraction from different cultures as quantified by NanoDrop spectrophotometry. Tum1 and Tum2 samples pertain to different tumouroid cultures, which were used in different bioreactor iterations.

	hUVEC	HepG2	Tum1	Tum2	Organoid
mRNA Concentration ($ng\,mL^{-1}$)	13.8	10.2	6.86	8.6	4.4
Absorbance at 260 nm (A260)	0.344	0.111	0.170	0.215	0.111
Absorbance at 280 nm (A280)	0.239	0.162	0.143	0.168	0.092
A260/280	1.44	1.57	1.18	1.28	1.21
A 260/230	0.19	0.41	0.19	0.18	0.13

tumouroids. As is shown in Figure 3.3, the largest organoids in culture had a diameter of roughly 700 µm, while tumouroids of 10k, 15k and 20k cells all had a diameter of over 1400 µm - more than double the size of the largest organoid. In fact, organoid size was more comparable to that of the 5k cells tumouroids, which measured around 400 µm in diameter, like some of the larger organoids seen in Figure 3.3 e).

3.3.3 Characterization of the generated tumouroids and organoids

mRNA expression analysis of tumouroids and organoids

The analysis of mRNA expression was aimed at assessing the presence of key genes. The presence of ITGB1, ITGB3, NOS3, COX-2, ETV2, KLF2 and RAP1 gene expression was assessed for 2D cultured hUVECs and for native liver, whereas the presence of HiF1-α, HGF, Ki-67, VEGF-A and ALB mRNA was tested for organoid, tumouroid and HepG2 cultures, as well as for native liver tissue. GAPDH expression was also tested for all conditions, serving as a loading control. Primers for all genes but HGF, ALB, VEGF-A and GAPDH, which were already present in the lab, were designed with the primer design tool of the National Center for Biotechnology Information of the U.S. National Institutes of Health [103].

Messenger RNA of tumouroid cultures and organoid cultures was harvested as described in subsection 2.4.3 and purified with DNAse treatment. mRNA of two-dimensional HepG2 and hUVEC cultures was also harvested, in order to observe changes in expression of target genes from 2D to 3D environments, and to get a positive control for angiogenesis, respectively. Two mRNA samples were made for tumouroids, since their protocol had been newly developed 'in-house'.

Full results of mRNA extraction, as quantified by NanoDrop spectrophotometry, can be seen in table 3.2. Detected mRNA concentration was very low for all samples, which is most likely due to the small sample size of 100k cells per condition. Small samples, in turn, were due to the fact that generation of large amounts of organoids and tumouroids is very resource- and time-consuming. Sample purity results, as shown by absorbance ratios, are also sub-par. Ideally, A260/A280 and A260/230 ratios would be around 2.1 and 1.8, respectively. The smaller values presented here show an abnormally high presence of proteins and especially of aromatic compounds mixed in the mRNA sample. The fact that mRNA isolation was performed with TRIzol reagent should be the main contributor for the exaggeratedly low A230/A260 ratio, since, as previously seen (subsection 3.1.1), aromatic compounds are mostly responsible for the absorbance of radiation with 230 nm wavelength. Furthermore, it is possible that the generally low concentrations of mRNA further propagated this effect, given that there may simply not have been enough

Table 3.3: Characterization of mRNA expression of different genes (left column) in samples (top column), as detected by polymerase chain reaction and gel electrophoresis. NT = Not Tested.

	hUVECs	Organoids	Tum1	Tum2	HepG2	Native Liver
ITGB1	Yes	NT	NT	NT	NT	Yes
ITGB3	Yes	NT	NT	NT	NT	Yes
NOS3	Yes	NT	NT	NT	NT	Yes
COX2	No	NT	NT	NT	NT	No
ETV2	No	NT	NT	NT	NT	No
KLF2	No	NT	NT	NT	NT	No
RAP1	Yes	NT	NT	NT	NT	Yes
HiF1-α	NT	Yes	Yes	No	Yes	Yes
HGF	NT	No	No	No	No	Yes
Ki-67	NT	No	No	No	No	No
GAPDH	Yes	Yes	Yes	Yes	Yes	Yes
VEGF	NT	No	No	No	Yes	No
ALB	NT	Yes	No	Yes	Yes	Yes

nucleic acid to fully compensate for measuring artifacts.

Nevertheless, these samples might be fit for their purpose, since they will later be amplified in PCR. Thus, the qualitative assessment of these samples regarding mRNA expression was continued.

Before analyzing the concrete results of the mRNA expression assay, one crucial consideration must be made: since this is the first time most of these primers are being used, as well as the first time that these systems (HepG2 tumouroids and human liver organoids) are being characterized, there is no reference point for what does or does not work. That is to say that, if a PCR product does appear in the expected place on the gel electrophoresis, it does not automatically mean that the mRNA is not expressed by the structure to which that specific PCR product pertained. It can be, for instance, that the primer was poorly designed, not well fabricated, faulty, or was somehow degraded before use; it could also be that the cells did in fact express that mRNA, but just not in sufficient quantity to allow for detection, or even that the collected sample was too small to present a meaningful amount of mRNA molecules. Furthermore, due to the volatile nature of RNA molecules, it might also be that these were degraded by RNAses that were not successfully inhibited by the RNAse Block solution, making it impossible for them to be transcribed into cDNA (and later amplified by PCR). If there were previous, robust characterizations of the samples that were tested in this work, comparing results might have allowed us to draw some conclusions regarding absence of results.

However, while negative results do not constitute definitive proof, positive results are very unlikely to be flukes. Since primers were designed to specifically target the desired genes, and PCR product length had been pre-determined by the primer design software, results found in the correct place are almost certainly valid. This is a result of base affinity phenomena of DNA molecules, the very principle on which polymerase chain reactions are based.

One must also keep in mind that a semi-quantitative analysis of mRNA expression is possible with these data, since the expression of target genes can be normalized through comparison with the expression of GAPDH. Thus, Figure 3.4 shows the results obtained in a semi-quantitative analysis of angiogenic genes

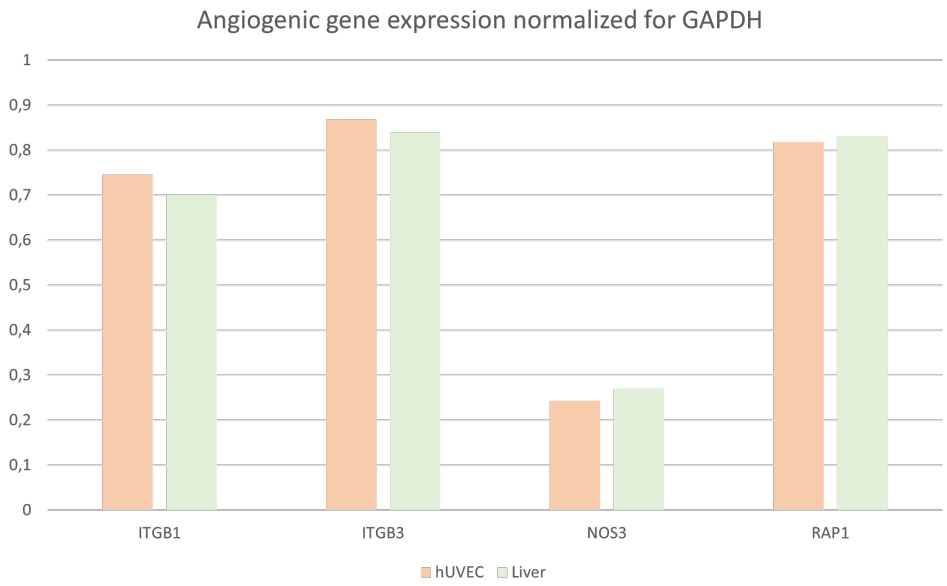

Figure 3.4: Semi-quantitative analysis of mRNA expression of detected angiogenic genes in hUVEC and liver samples, normalized for GAPDH expression.

in liver and hUVEC samples, while Figure 3.5 compares the expression levels of key genes in hepatic function between liver, organoid, tumouroid, and HepG2 samples.

As can be seen in Figure 3.4, ITGB1, ITGB3, NOS3 and RAP1 genes are expressed in an identical manner in liver and in hUVEC culture, while the expression of COX2, ETV2 and KLF2 was not detected in either. Table 3.3 shows that HiF1-α expression was detected in all samples but one (Tum2), as well as ALB expression (which was not detected in Tum1), and HGF mRNA was detected only in the liver sample, while VEGF was only detected o be expressed by 2D HepG2 cultures. However, a closer look at the semi-quantitative results represented in Figure 3.5 shows that there is a great disparity in expression levels of these genes among samples. Ki-67 expression was ubiquitously undetected, while GAPDH mRNA was always present.

In an initial analysis, it is interesting to see the differential expression between organoids and native liver, which are quite similar, except in that the latter, unlike the former, expresses the HGF gene. A similar result can be seen when comparing tumouroid samples Tum1 and Tum2 to the liver sample, although Tum1 and Tum2 express either HiF1-α or ALB, but not both at the same time. In fact, these tumouroid samples are different in origin, since Tum1 mRNA was obtained from tumouroids with 10k cells each, while Tum2 mRNA was derived from smaller tumouroids, each with 5k cells. The fact that there is differential gene expression within the same sample type is and indicator that tumouroids might not all show the same behaviour, and that said behaviour can be related to the size of the structure. Another interesting comparison can be made between tumouroids and organoids - while both types of structures do not show expression of VEGF, Ki-67 and HGF, they are capable of expression of HiF1-α and ALB. Differential expression can only be seen in that tumouroid cultures have not shown to be capable of simultaneous expression of both ALB and HiF1-α. However, it is important to note that this might not be a direct result of the nature of the cells, since organoid cultures were conditioned with specific medium in order to stimulate

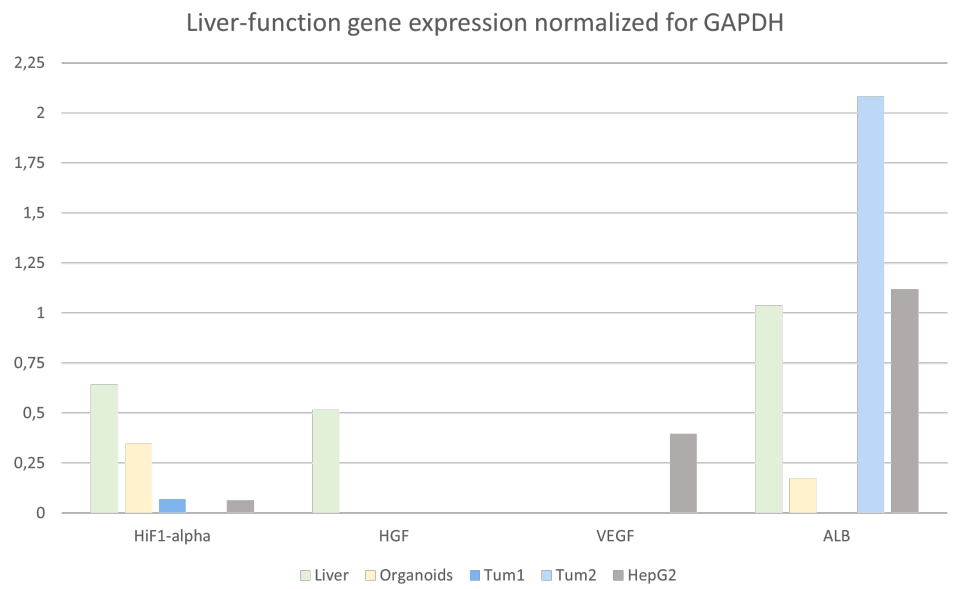

Figure 3.5: Semi-quantitative analysis of mRNA expression of detected liver function-related genes in organoid, tumouroid, HepG2 and liver samples, normalized for GAPDH expression.

the expression of liver-related genes, whereas tumouroid cultures were grown in unspecific medium. One last important consideration regards the change in expression that occurs when HepG2 cells go from a two-dimensional organization to forming a three-dimensional structure. Indeed, HepG2 cells in 2D culture were shown to express VEGF as well as HiF1-α and ALB, which did not happen for tumouroid cultures, which exclusively expressed ALB or HiF1-α and did not express VEGF. The change in cellular architecture seems therefore to directly influence gene expression, since all other conditions were kept between both cultures. Remarkably, 3D-cultured tumouroids have an expression profile more akin to that of a native liver than 2D HepG2 cultures, further suggesting that 3D cell culturing more closely resembles physiological environments. GAPDH expression in all samples proves a successful trial and ads robustness to the results, serving as a positive control for the experimental procedure.

The results discussed above become even more meaningful when the roles of genes are analysed, both in general and in the context of angiogenesis.

The Integrin Subunit Beta 1 (ITGB1) gene is associated with the VEGF signaling pathway, which in turn is deeply interconnected with angiogenesis phenomena, whereas Integrin Subunit Beta 3 (ITGB3) in endothelial cells is a key gene in the migration and angiogenic processes [113, 114]. The Nitric Oxide Synthase 3 (NOS3) gene is partially responsible for the synthesis of nitric oxide, a compound with a multitude of roles in the vascular system [115]. Lastly, the RAP1 gene codes for a protein necessary for VEGF-dependent angiogenesis in endothelial cells [116]. The expression of these genes in hUVECs, as well as in liver tissue, attests to their capability for angiogenesis. Furthermore, the fact that angiogenesis-related genes are expressed by the liver further reinforces the need for co-culture of liver cells with endothelial cells for the development of an accurate liver model.

Next, the gene coding for cyclooxygenase-2 (COX-2 or COX2) has been shown to be involved in the angiogenesis and proliferation of certain types of GI tract tumours, while ETS Variant Transcription Factor

2 (ETV2) is a transcription factor required for tumour angiogenesis[117, 118, 119]. Since the sample of liver tissue was harvested from a healthy liver, and the culture from which hUVECs were harvested are not tumorigenic, it is understandable that the expression of COX2 and ETV2 were not detected. Analogously, Kruppel Like Factor 2 (KLF2), which encodes proteins are zinc finger proteins involved in a plethora of processes, ranging from adipogenesis to inflammation, with an inhibitory role against VEGF-A, has no detected expression in healthy, angiogenic tissues [120].

The Hypoxia Inducible Factor 1 Subunit Alpha (HiF1-1α) gene codes for the alpha subunit of transcription factor hypoxia-inducible factor-1 (HIF-1), a regulator of cell behaviour as a response to hypoxia. The Hepatocyte growth factor (HGF) gene codes for a transcription factor with angiogenic, tumorigenic and tissue regeneration roles [121, 122]. What is most notable to see, regarding both of these genes, is the absence of constant expression in spheroids, which are typically hypoxic structures. Organoids, despite expressing HiF1-1α, do not express HGF, unlike the liver; the same pattern can be seen for the expression of those genes in tumouroids, albeit aggravated by the exclusive expression of HiF1-1α or ALB. Differential expression when compared to the liver might be due to the fact that the organoids and tumouroids might still be immature in these culture conditions. It is also a possibility that HGF and HiF-1α expression is dependent on contact or co-culture with other non-parenchymal liver cell types, such as hepatoblasts or fibroblasts, given their role in tissue regeneration processes. This hypothesis can be tested in another study, by co-culture of multiple liver cell types, by close examination of the pathways associated with each gene, or by combining both of these methods.

The Ki-67 gene is a traditional cancer and proliferation marker, ideal for the study of tumorigenic activity [123]. Given its role, it is intriguing that Ki-67 expression was not detected neither in HepG2 nor in tumouroid samples. In fact, a closer look at the full results of the PCR reveals that an amplification product was detected in the trial for Ki-67 amplification, but was discarded due to not having the appropriate size. One possibility for this outcome, besides the lack of expression of the gene by the cells, is contamination, either with another type of DNA molecule for which the primers have more affinity, or with an enzyme that digested the products of the polymerase chain reaction. Another possible explanation is the amplification of "background noise", which can have occurred in a semi-random fashion.

The Albumin gene (ALB) codes for albumin, the most abundant protein in the blood, which is typically synthesized in the liver, serving as a marker of liver function [124]. Notably, albumin-precursor mRNA was detected in all liver-like structures, further solidifying the possibility of using them as a model for liver function. The Vascular Endothelial Growth Factor A gene (VEGF-A, here abbreviated to VEGF) codes for a growth factor heavily implicated in angiogenic processes, stimulating proliferation and migration of endothelial cells. VEGF has been shown to be required for angiogenesis, both in physiological and pathological states. Thus, it is of no surprise to see that it is indeed expressed in HepG2 cells, which are known for their pro-angiogenic behaviour [125]. Interestingly, however, HepG2 cells organized in tumouroids do not show signs of VEGF expression.

Lastly, the glyceraldehyde-3-phosphate dehydrogenase (GAPDH) gene serves as a reference gene, since it is constitutively active in normal cell behaviour. Although the positive control of the experiment indicates a successful assay, the data obtained in this experiment would meaningfully increase in signifi-

cance with replicates, which could disprove or corroborate the results seen in this section. Given that the procedure for the characterization of the 6 samples mentioned above was only carried out once, it is possible that it does not constitute a statistically relevant result. To solve this caveat, the only possible solution is to repeat the exact same procedure with different samples obtained from structures in the same conditions, and compare results of different runs.

Although the previously obtained results are fit for the current purpose, there are some possibilities to achieve even more meaningful ones. First and foremost, quantitative analysis of mRNA expression, in combination with qualitative analysis, might provide a deeper insight into the behaviour of the cell culture. If, for example, hypoxia-related genes are only produced by a small amount of cells, it might be the case that nutrient diffusion is not being equally effectively in reaching all cells. Furthermore, these results merely characterize mRNA production, which is subject to degradation and splicing. To circumvent this limitation, a characterization of the proteins present in each culture can be done, via immunohistochemistry. Possible assays to include in said characterization are the Western blot, which is simple in its execution, or immunofluorescence assays on histological preparations, which allow for the characterization of the protein's location inside the cell/spheroid/organoid. Lastly, and perhaps most importantly, these same assays will become much more significant once they can also be applied to three-dimensional, microfluidic-based, dynamic cultures, as the ones described below. Currently, some technical limitations are preventing this outcome, which will be discussed with detail in section 3.4.2.

3.4 Dynamic cultures in a continuous flow bioreactor

3.4.1 Liver-free angiogenic assays

In liver-free angiogenic assays, a co-culture of hUVECs and hMSCs was carried out in a 80/20 proportion, with a complete absence of liver organoids and tumouroids, in either Matrigel® or in our dECM-based fibrin hydrogel. The goal of the experiment was to test whether angiogenesis was possible in a 3D, microfluidic environment, with as little interference of angiogenesis-unrelated structures as possible.

Culture systems with Matrigel® as the supporting hydrogel were not shown to be capable of *de novo* angiogenic formation. In fact, these results are in line with those previously obtained in the lab, with a similar microfluidic system. In itself, the lack of angiogenesis is rather surprising, since tube formation assays on Matrigel® have been thoroughly studied and characterized [126].

On the other hand, tube formation assays carried out in fibrin-based dECM hydrogels led to microvascular structures in 66% of the cases. Well-defined, extensive branching networks of blood vessel-like structures can be seen spread out throughout the central chamber of the microfluidic chips (Figure 3.6 b) and c)). This result is of the utmost importance, since it establishes that our current system is capable of angiogenesis, providing the necessary proof-of-concept for advancing into the next stage, which is the vascularization of hepatic structures. Furthermore, the fact that angiogenesis was seen in more than one trial solidifies the capabilities of the system to consistently generate vascular networks. It is also important to note that formation of microvasculature in the central chamber did not occur on the same culture day,

with one bioreactor system showing signs of *de novo* angiogenesis as early as day 1 in culture, whereas the other successful bioreactor culture only showed vessel formation starting at day 5. Vessel formation, as hypothesized, was aided by the stress conditions caused by absence of flow for periods of 24 hours.

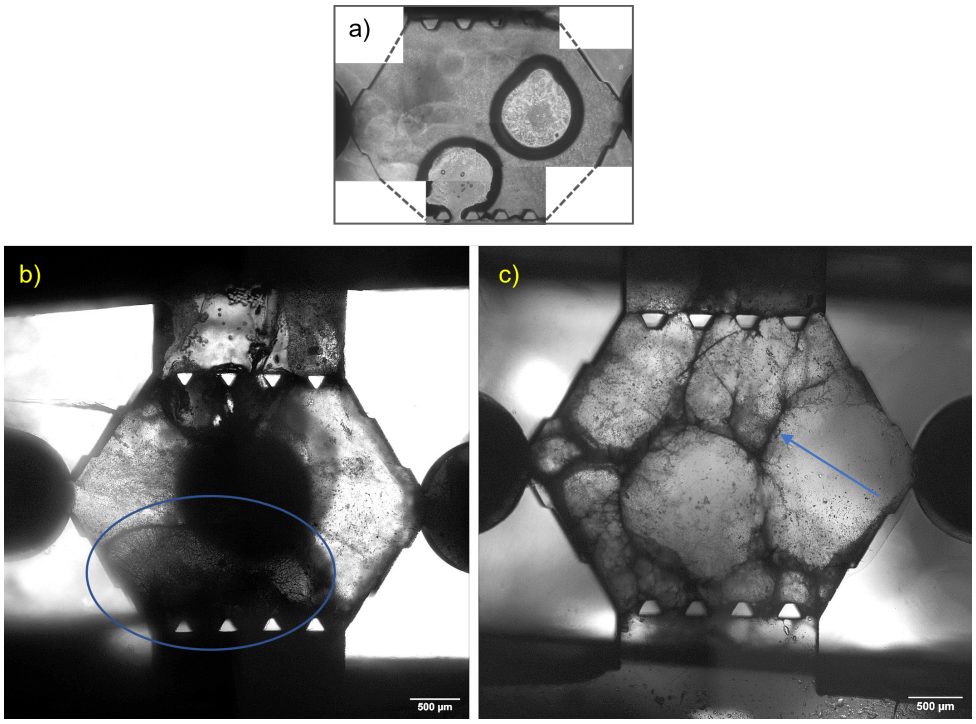

Figure 3.6: Brightfield imaging of liver-free angiogenic assays. a) Angiogenic liver-free culture 1 day after the start of medium perfusion. b) First trial with successful formation of a microvascular network (highlighted with ellipse) inside the central chamber of the device (culture day 11). c) Second successful angiogenesis trial in a liver-free setup, with the formation of microscopic vessels (highlighted with blue arrow) (culture day 13). Scale bar = 500 µm.

In comparing the results from the dECM-based hydrogel with those obtained for Matrigel® , it becomes clear that the use of the dECM-based fibrin hydrogel developed in the lab is a key factor in the stimulation of angiogenic behaviour. Indeed, Matrigel® , as good as it may be for static cell culturing and angiogenic assays, might simply not be suited for this system. The reasons for this behaviour are not yet clear, and might be a good object for a future study. Main key points to be analysed regarding Matrigel® behaviour in a microfluidic setting would be the impact of down-scaling on the gel's porosity and mechanical properties. Furthermore, Matrigel® is a generic, xenogeneic hydrogel, derived from mouse sarcoma tumour. Meanwhile, our dECM-based hydrogel can be adapted to be xenogeneic-free, is specific for liver matrix, which is highly angiogenic, and can have its mechanical properties adjusted by variation of the degree of cross-linking between fibrin chains. Here, it was shown that our dECM-based hydrogel, in combination with the microfluidic chip that was also designed in our laboratory, is capable of supporting tube formation by hUVEC/hMSC co-cultures, opening the door for the creation of vascularized organ models in a microfluidic system.

3.4.2 Tumouroid and Organoid angiogenic assays

In angiogenic trials with hepatic structures, a similar setup was followed as the one used for liver-free angiogenic assays, with the differences that the gel substrate used was always dECM-based, and that tumouroids or organoids were incorporated in the hydrogel alongside hUVECs and hMSCs. 4 trials were made for the formation of microvascular networks in environments with tumouroid presence, with proportions and numbers of incorporated spheroids as shown in Table 2.4. Only one trial was made for the neovascularization of organoids, for which the number of organoid structures was not previously counted, in order for them to maintain as much structural integrity as possible. Another deviation from the liver-free protocol that was incorporated in the microfluidic culture of organoids was the use of 50/50 angiogenic/organoid medium, with the rationale of combining angiogenesis and organoid support. Whenever a component was present in both media formulations, the highest concentration was used. A step-wise description of the bioreactor setup procedure can be found in Figure **??**.

3.5 Possible improvements and future prospects

Chapter 4

Conclusion

Liver disease is a public health problem responsible for over 3.5% (2 million) of all deaths per year, worldwide [4]. Furthermore, patients affected by liver disease show an increased probability of being affected by other comorbidities and of being socioeconomically set back due to their medical conditions. However, novel therapies can only be developed once the behaviour of the organ is progressively and deeply understood, both in physiological and diseased conditions. For this, it is crucial to have accurate models of healthy and damaged liver behaviour that can be utilized to gain useful insight on liver mechanisms or to test novel therapeutic approaches against liver disease. In this work, we lay the foundation for the production of a vascularized, three-dimensional model for healthy and cancerous liver in a microfluidic setting.

This thesis based itself on the current state-of-the-art in hydrogel-, microfluidics- and organoid applications, as well as on previous research conducted in our lab, to successfully stimulate *de novo* angiogenesis. To do so, hUVECs and hMSCs grown in two-dimensional cultures were incorporated in a bioreactor setup with continuous flow driven by a peristaltic pump, where they were cultured with angiogenic medium and formed an interconnected microvascular network in two out of three trials. Besides constituting the foundation for further work, this result validates the dECM-based hydrogel and the microfluidic chip used in the bioreactor system, which were both developed in our lab.

These principles were then applied to try and generate a culture of vascularized liver organoids and tumouroid. Characterization of mRNA expression showed that organoids and tumouroids expressed some, but not all of the markers seen in native liver. These hepatic spheroids, which had previously been expanded in 3D culture, were incorporated into the microfluidic platform alongside hUVECs and hMSCs. In all five performed trials (four with tumouroid cultures and one with an organoid culture), it was not possible to see signs of robust angiogenesis, unlike what happened in liver-free cultures. However, this does not directly denote that blood vessel formation is impossible under these conditions, since the protocol was optimized on a trial-and-error basis, and has a multitude of caveats that, despite having already been identified, have not yet been filled.

The technology developed in this project can be used to lay the foundation for the development of a model for healthy and cancerous human liver, which can in turn be used in high-throughput screening

applications, be transplanted into animals or scaled up for possible therapeutic approaches. If these applications prove to be successful, the technology used in this work can be modified to be used in other spheroid-capable tissues, such as kidney and pancreas.

Bibliography

[1] S. K. Sarin and R. Maiwall. *Global Burden Of Liver Disease: A True Burden On Health, Sciences and Economies*. URL: https://www.worldgastroenterology.org/publications/e-wgn/e-wgn-expert-point-of-view-articles-collection/global-burden-of-liver-disease-a-true-burden-on-health-sciences-and-economies (visited on 09/22/2021).

[2] M. Melato, F. Sasso, and F. Zanconati. "Liver cirrhosis and liver cancer. A study of their relationship in 2563 autopsies." In: *Zentralbl Pathol.* 139.1 (1993), pp. 25–30.

[3] YS. Lim and WR. Kim. "The global impact of hepatic fibrosis and end-stage liver disease." In: *Clin Liver Dis.* 12.4 (2008), pp. 733–46. DOI: 10.1016/j.cld.2008.07.00.

[4] S.K. Asrani et al. "Burden of liver diseases in the world." In: *J Hepatol.* 70.1 (2019), pp. 151–171. DOI: 10.1016/j.jhep.2018.09.014.

[5] S. K. Sarin and R. Maiwall. *Global Burden Of Liver Disease: A True Burden On Health, Sciences and Economies, Part II*. URL: https://www.worldgastroenterology.org/publications/e-wgn/e-wgn-expert-point-of-view-articles-collection/global-burden-of-liver-disease-a-true-burden-on-health-sciences-and-economies (visited on 09/22/2021).

[6] W. Ray Kim et al. "Burden of liver disease in the United States: Summary of a workshop". In: *Hepatology* 36.1 (2002), pp. 227–242. DOI: https://doi.org/10.1053/jhep.2002.34734. eprint: https://aasldpubs.onlinelibrary.wiley.com/doi/pdf/10.1053/jhep.2002.34734. URL: https://aasldpubs.onlinelibrary.wiley.com/doi/abs/10.1053/jhep.2002.34734.

[7] A.F. Peery et al. "Burden and Cost of Gastrointestinal, Liver, and Pancreatic Diseases in the United States: Update 2018." In: *Gastroenterology* 156.1 (2019), pp. 254–272. DOI: 10.1053/j.gastro.2018.08.063.

[8] Maria Stepanova et al. "Direct and indirect economic burden of chronic liver disease in the United States". In: *Clinical Gastroenterology and Hepatology* 15.5 (2017), pp. 759–766.

[9] Sunmi Lee, Woojin Chung, and Kyung-Rae Hyun. "Socioeconomic costs of liver disease in Korea". In: *The Korean journal of hepatology* 17.4 (2011), p. 274.

[10] Trading Economics. *South Korea GDP*. URL: https://tradingeconomics.com/south-korea/gdp (visited on 09/22/2021).

[11] Pierre-Antoine Soret et al. "In Vitro and In Vivo Models of Non-Alcoholic Fatty Liver Disease: A Critical Appraisal". In: *Journal of Clinical Medicine* 10.1 (2021), p. 36.

[12] Tanja Cvitanović et al. “Large-scale computational models of liver metabolism: How far from the clinics?” In: *Hepatology* 66.4 (2017), pp. 1323–1334.

[13] Michela Anna Polidoro et al. “Experimental liver models: From cell culture techniques to microfluidic organs-on-chip”. In: *Liver International* 41.8 (2021), pp. 1744–1761.

[14] Yan Liu et al. “Animal models of chronic liver diseases”. In: *American Journal of Physiology-Gastrointestinal and Liver Physiology* 304.5 (2013), G449–G468.

[15] Vahid Hosseini et al. “Current progress in hepatic tissue regeneration by tissue engineering”. In: *Journal of translational medicine* 17.1 (2019), pp. 1–24.

[16] Vasimahmed Lala et al. “Liver function tests”. In: *StatPearls [Internet]* (2020).

[17] AJ Knell. “Liver function and failure: the evolution of liver physiology”. In: *Journal of the Royal College of Physicians of London* 14.3 (1980), p. 205.

[18] Romil Saxena, Neil D Theise, and James M Crawford. “Microanatomy of the human liver—exploring the hidden interfaces”. In: *Hepatology* 30.6 (1999), pp. 1339–1346.

[19] Arjun Kalra et al. “Physiology, liver”. In: (2018).

[20] Anna Stenvall et al. “A small-scale anatomical dosimetry model of the liver”. In: *Physics in Medicine & Biology* 59.13 (2014), p. 3353.

[21] Kirstin H. *Dr. Das: Liver1 Flashcards*. URL: https://www.chegg.com/flashcards/dr-das-liver1-c4ae4960-9019-4de7-959f-9a05f530cc52/deck (visited on 10/17/2021).

[22] *Liver cancer - Symptoms and causes*. URL: https://www.mayoclinic.org/diseases-conditions/liver-cancer/symptoms-causes/syc-20353659 (visited on 10/18/2021).

[23] Irfan Ahmed and Dileep N Lobo. “Malignant tumours of the liver”. In: *Surgery (Oxford)* 27.1 (2009), pp. 30–37.

[24] Anila Kumar, Bashar Sharma, and Hrishikesh Samant. “Liver angiosarcoma”. In: *StatPearls [Internet]*. StatPearls Publishing, 2020.

[25] Ju Dong Yang et al. “A global view of hepatocellular carcinoma: trends, risk, prevention and management”. In: *Nature reviews Gastroenterology & hepatology* 16.10 (2019), pp. 589–604.

[26] Detlef Schuppan and Nezam H Afdhal. “Liver cirrhosis”. In: *The Lancet* 371.9615 (2008), pp. 838–851.

[27] Gregory T Everson. “Management of cirrhosis due to chronic hepatitis C”. In: *Journal of hepatology* 42.1 (2005), S65–S74.

[28] Jules L Dienstag et al. “Histological outcome during long-term lamivudine therapy”. In: *Gastroenterology* 124.1 (2003), pp. 105–117.

[29] Yun-Fan Liaw et al. “Lamivudine for patients with chronic hepatitis B and advanced liver disease”. In: *New England Journal of Medicine* 351.15 (2004), pp. 1521–1531.

[30] U.S. Department of Veteran Affairs. *FAQ: What is the survival rate after a liver transplant?* URL: https://www.hepatitis.va.gov/liver-transplant/patient/faqs/ (visited on 10/19/2021).

[31] *Global Observatory on Donation and Transplantation*. URL: www.transplant-observatory.org. (visited on 10/19/2021).

[32] Rafael Matesanz et al. “How Spain reached 40 deceased organ donors per million population”. In: *American journal of transplantation* 17.6 (2017), pp. 1447–1454.

[33] James F Trotter and Andrés Cárdenas. *Liver transplantation around the world*. 2016.

[34] Vasimahmed Lala et al. “Liver function tests”. In: *StatPearls [Internet]* (2020).

[35] Minjun Chen et al. “Drug-induced liver injury: Interactions between drug properties and host factors”. In: *Journal of hepatology* 63.2 (2015), pp. 503–514.

[36] Tsuyoshi Yokoi and Shingo Oda. “Models of idiosyncratic drug-induced liver injury”. In: *Annual Review of Pharmacology and Toxicology* 61 (2021), pp. 247–268.

[37] Michela Anna Polidoro et al. “Experimental liver models: From cell culture techniques to microfluidic organs-on-chip”. In: *Liver International* 41.8 (2021), pp. 1744–1761.

[38] Patricio Godoy et al. “Recent advances in 2D and 3D in vitro systems using primary hepatocytes, alternative hepatocyte sources and non-parenchymal liver cells and their use in investigating mechanisms of hepatotoxicity, cell signaling and ADME”. In: *Archives of toxicology* 87.8 (2013), pp. 1315–1530.

[39] M José Gómez-Lechón et al. “Competency of different cell models to predict human hepatotoxic drugs”. In: *Expert opinion on drug metabolism & toxicology* 10.11 (2014), pp. 1553–1568.

[40] Daniela Deharde et al. “Bile canaliculi formation and biliary transport in 3D sandwich-cultured hepatocytes in dependence of the extracellular matrix composition”. In: *Archives of toxicology* 90.10 (2016), pp. 2497–2511.

[41] Sarah M Maritan, Eric Y Lian, and Lois M Mulligan. “An efficient and flexible cell aggregation method for 3D spheroid production”. In: *Journal of visualized experiments: JoVE* 121 (2017).

[42] Catherine C Bell et al. “Characterization of primary human hepatocyte spheroids as a model system for drug-induced liver injury, liver function and disease”. In: *Scientific reports* 6.1 (2016), pp. 1–13.

[43] Fuyin Zheng et al. “Organ-on-a-Chip Systems: microengineering to biomimic living systems”. In: *Small* 12.17 (2016), pp. 2253–2282.

[44] Christopher J Hindley, Lucıa Cordero-Espinoza, and Meritxell Huch. “Organoids from adult liver and pancreas: stem cell biology and biomedical utility”. In: *Developmental biology* 420.2 (2016), pp. 251–261.

[45] Gabriel Benton et al. “Matrigel: from discovery and ECM mimicry to assays and models for cancer research”. In: *Advanced drug delivery reviews* 79 (2014), pp. 3–18.

[46] Alessandra Merenda, Nicola Fenderico, and Madelon M Maurice. “Wnt signaling in 3D: recent advances in the applications of intestinal organoids”. In: *Trends in cell biology* 30.1 (2020), pp. 60–73.

[47] Cody J Aros, Carla J Pantoja, and Brigitte N Gomperts. “Wnt signaling in lung development, regeneration, and disease progression”. In: *Communications biology* 4.1 (2021), pp. 1–13.

[48] Shiro Yui et al. “Functional engraftment of colon epithelium expanded in vitro from a single adult Lgr5+ stem cell”. In: *Nature medicine* 18.4 (2012), pp. 618–623.

[49] Meritxell Huch et al. “In vitro expansion of single Lgr5+ liver stem cells induced by Wnt-driven regeneration”. In: *Nature* 494.7436 (2013), pp. 247–250.

[50] Meritxell Huch et al. “Long-term culture of genome-stable bipotent stem cells from adult human liver”. In: *Cell* 160.1-2 (2015), pp. 299–312.

[51] Kerstin Schneeberger et al. “Large-scale production of LGR5-positive bipotential human liver stem cells”. In: *Hepatology* 72.1 (2020), pp. 257–270.

[52] Takanori Takebe et al. “Vascularized and functional human liver from an iPSC-derived organ bud transplant”. In: *Nature* 499.7459 (2013), pp. 481–484.

[53] Akihiro Asai et al. “Paracrine signals regulate human liver organoid maturation from induced pluripotent stem cells”. In: *Development* 144.6 (2017), pp. 1056–1064.

[54] Yuan Guan et al. “Human hepatic organoids for the analysis of human genetic diseases”. In: *JCI insight* 2.17 (2017).

[55] MP Lutolf and JA Hubbell. “Synthetic biomaterials as instructive extracellular microenvironments for morphogenesis in tissue engineering”. In: *Nature biotechnology* 23.1 (2005), pp. 47–55.

[56] Martin Ehrbar et al. “Biomolecular hydrogels formed and degraded via site-specific enzymatic reactions”. In: *Biomacromolecules* 8.10 (2007), pp. 3000–3007.

[57] Shicheng Ye et al. “A chemically defined hydrogel for human liver organoid culture”. In: *Advanced Functional Materials* 30.48 (2020), p. 2000893.

[58] Sandro Nuciforo and Markus H Heim. “Organoids to model liver disease”. In: *JHEP Reports* 3.1 (2021), p. 100198.

[59] Yuan Guan et al. “Human hepatic organoids for the analysis of human genetic diseases”. In: *JCI insight* 2.17 (2017).

[60] Raj Vuppalanchi and Naga Chalasani. “Nonalcoholic fatty liver disease and nonalcoholic steatohepatitis: Selected practical issues in their evaluation and management”. In: *Hepatology* 49.1 (2009), pp. 306–317.

[61] Željko Reiner et al. “Lysosomal acid lipase deficiency–an under-recognized cause of dyslipidaemia and liver dysfunction”. In: *Atherosclerosis* 235.1 (2014), pp. 21–30.

[62] A Dash et al. “Pharmacotoxicology of clinically-relevant concentrations of obeticholic acid in an organotypic human hepatocyte system”. In: *Toxicology in Vitro* 39 (2017), pp. 93–103.

[63] Shuyong Wang et al. “Human ESC-derived expandable hepatic organoids enable therapeutic liver repopulation and pathophysiological modeling of alcoholic liver injury”. In: *Cell research* 29.12 (2019), pp. 1009–1026.

[64] Yun-Zhong Nie et al. “Recapitulation of hepatitis B virus–host interactions in liver organoids from human induced pluripotent stem cells”. In: *EBioMedicine* 35 (2018), pp. 114–123.

[65] Sheng He et al. “PDXliver: a database of liver cancer patient derived xenograft mouse models”. In: *BMC cancer* 18.1 (2018), pp. 1–9.

[66] Juliane Friemel et al. “Intratumor heterogeneity in hepatocellular carcinoma”. In: *Clinical Cancer Research* 21.8 (2015), pp. 1951–1961.

[67] Zuzana Macek Jilkova, Keerthi Kurma, and Thomas Decaens. “Animal models of hepatocellular carcinoma: the role of immune system and tumor microenvironment”. In: *Cancers* 11.10 (2019), p. 1487.

[68] Jarno Drost and Hans Clevers. “Organoids in cancer research”. In: *Nature Reviews Cancer* 18.7 (2018), pp. 407–418.

[69] Laura Broutier et al. “Human primary liver cancer–derived organoid cultures for disease modeling and drug screening”. In: *Nature medicine* 23.12 (2017), pp. 1424–1435.

[70] Sandro Nuciforo et al. “Organoid models of human liver cancers derived from tumor needle biopsies”. In: *Cell reports* 24.5 (2018), pp. 1363–1376.

[71] Anna Saborowski et al. “Murine liver organoids as a genetically flexible system to study liver cancer in vivo and in vitro”. In: *Hepatology communications* 3.3 (2019), pp. 423–436.

[72] HIMEDIA. URL: https://himedialabs.com/intl/en/products/Animal-Cell-Culture/Cell-Culture-Tested-Chemicals-Attachment-factors/Gelatin-TC041 (visited on 09/26/2021).

[73] ThermoFisher Scientific. URL: https://www.thermofisher.com/es/es/home/life-science/cell-culture/organoids-spheroids-3d-cell-culture/extracellular-matrices-ecm/collagen-i-rat-bovine.html (visited on 09/26/2021).

[74] Corning. URL: https://www.corning.com/worldwide/en/products/life-sciences/products/surfaces/ultra-low-attachment-surface.html (visited on 09/26/2021).

[75] Indira Padmalayam and Mark J Suto. “3D cell cultures: mimicking in vivo tissues for improved predictability in drug discovery”. In: *Annual Reports in Medicinal Chemistry* 47 (2012), pp. 367–378.

[76] Zuzana Koledova. “3D Cell Culture: An Introduction”. In: *3D Cell Culture: Methods and Protocols*. Ed. by Zuzana Koledova. New York, NY: Springer New York, 2017, pp. 1–11. ISBN: 978-1-4939-7021-6. DOI: 10.1007/978-1-4939-7021-6_1. URL: https://doi.org/10.1007/978-1-4939-7021-6_1.

[77] *Three-Dimensional (3D) Cell Culture (Microphysiological) Platforms as Drug Development Tools*. U.S.F.D.A. URL: https://www.fda.gov/drugs/regulatory-science-action/three-dimensional-3d-cell-culture-microphysiological-platforms-drug-development-tools (visited on 09/26/2021).

[78] Ramsey Foty. “A simple hanging drop cell culture protocol for generation of 3D spheroids”. In: *Journal of visualized experiments: JoVE* 51 (2011).

[79] Wenda Wang, Ravin Narain, and Hongbo Zeng. “Hydrogels”. In: *Polymer Science and Nanotechnology*. Elsevier, 2020, pp. 203–244.

[80] Fiona Stapleton et al. “Silicone hydrogel contact lenses and the ocular surface”. In: *The ocular surface* 4.1 (2006), pp. 24–43.

[81] Ibrahim M El-Sherbiny and Magdi H Yacoub. “Hydrogel scaffolds for tissue engineering: Progress and challenges”. In: *Global Cardiology Science and Practice* 2013.3 (2013), p. 38.

[82] Danielle Lynne Taylor and Marc in het Panhuis. “Self-healing hydrogels”. In: *Advanced Materials* 28.41 (2016), pp. 9060–9093.

[83] Erwin Kuntz and Hans-Dieter Kuntz. *Hepatology, Principles and practice: history, morphology, biochemistry, diagnostics, clinic, therapy*. Springer Science & Business Media, 2006.

[84] Shicheng Ye et al. “Hydrogels for liver tissue engineering”. In: *Bioengineering* 6.3 (2019), p. 59.

[85] A Martinez-Hernandez and PS Amenta. “The hepatic extracellular matrix. II. Ontogenesis, regeneration and cirrhosis.” In: *Virchows Archiv. A, Pathological anatomy and histopathology* 423.2 (1993), pp. 77–84.

[86] Pierre Bedossa and Valérie Paradis. “Liver extracellular matrix in health and disease”. In: *The Journal of Pathology: A Journal of the Pathological Society of Great Britain and Ireland* 200.4 (2003), pp. 504–515.

[87] Chunxia Zhu et al. “Liver progenitor cell interactions with the extracellular matrix”. In: *Journal of tissue engineering and regenerative medicine* 7.10 (2013), pp. 757–766.

[88] Sheva Naahidi et al. “Biocompatibility of hydrogel-based scaffolds for tissue engineering applications”. In: *Biotechnology advances* 35.5 (2017), pp. 530–544.

[89] Lakshmi S Nair and Cato T Laurencin. “Biodegradable polymers as biomaterials”. In: *Progress in polymer science* 32.8-9 (2007), pp. 762–798.

[90] Junmin Zhu and Roger E Marchant. “Design properties of hydrogel tissue-engineering scaffolds”. In: *Expert review of medical devices* 8.5 (2011), pp. 607–626.

[91] Jérémy Bomo et al. “Increasing 3D matrix rigidity strengthens proliferation and spheroid development of human liver cells in a constant growth factor environment”. In: *Journal of Cellular Biochemistry* 117.3 (2016), pp. 708–720.

[92] Nasim Annabi et al. “Controlling the porosity and microarchitecture of hydrogels for tissue engineering”. In: *Tissue Engineering Part B: Reviews* 16.4 (2010), pp. 371–383.

[93] Seema S Desai et al. “Physiological ranges of matrix rigidity modulate primary mouse hepatocyte function in part through hepatocyte nuclear factor 4 alpha”. In: *Hepatology* 64.1 (2016), pp. 261–275.

[94] Anuj Tripathi and Jose Savio Melo. “Preparation of a sponge-like biocomposite agarose–chitosan scaffold with primary hepatocytes for establishing an in vitro 3D liver tissue model”. In: *RSC Advances* 5.39 (2015), pp. 30701–30710.

[95] Xiaohong Wang and Chang Liu. “Fibrin hydrogels for endothelialized liver tissue engineering with a predesigned vascular network”. In: *Polymers* 10.10 (2018), p. 1048.

[96] George M Whitesides. “The origins and the future of microfluidics”. In: *nature* 442.7101 (2006), pp. 368–373.

[97] Francesca Bragheri, Rebeca Martınez Vázquez, and Roberto Osellame. “Microfluidics”. In: *Three-Dimensional Microfabrication Using Two-Photon Polymerization*. Elsevier, 2020, pp. 493–526.

[98] Jing Wu and Min Gu. “Microfluidic sensing: state of the art fabrication and detection techniques”. In: *Journal of biomedical optics* 16.8 (2011), p. 080901.

[99] Omer Nur and Magnus Willander. “Chapter 3 - Conventional nanofabrication methods”. In: *Low Temperature Chemical Nanofabrication*. Ed. by Omer Nur and Magnus Willander. Micro and Nano Technologies. William Andrew Publishing, 2020, pp. 49–86. ISBN: 978-0-12-813345-3. DOI: https://doi.org/10.1016/B978-0-12-813345-3.00003-4. URL: https://www.sciencedirect.com/science/article/pii/B9780128133453000034.

[100] *Introduction to PDMS soft-lithography and polymer molding for microfluidics*. ELVEFLOW. URL: https://www.elveflow.com/microfluidic-reviews/soft-lithography-microfabrication/introduction-about-soft-lithography-and-polymer-molding-for-microfluidic/ (visited on 10/31/2021).

[101] Eiji Takahashi. “Anoxic cell core can promote necrotic cell death in cardiomyocytes at physiological extracellular PO2”. In: *American Journal of Physiology-Heart and Circulatory Physiology* 294.6 (2008), H2507–H2515.

[102] *ATCC: The Global Bioresource Center*. ATCC. URL: https://www.atcc.org/ (visited on 06/21/2021).

[103] *Primer-BLAST*. NCBI. URL: https://www.ncbi.nlm.nih.gov/tools/primer-blast/ (visited on 10/14/2021).

[104] Keren Bellacen and Eli C Lewis. “Aortic ring assay”. In: *JoVE (Journal of Visualized Experiments)* 33 (2009), e1564.

[105] *NanoDrop Protein Quantification*. ThermoFisher. URL: https://www.thermofisher.com/pt/en/home/industrial/spectroscopy-elemental-isotope-analysis/molecular-spectroscopy/ultraviolet-visible-visible-spectrophotometry-uv-vis-vis/uv-vis-vis-instruments/nanodrop-microvolume-spectrophotometers/nanodrop-protein-quantification.html (visited on 10/28/2021).

[106] *NanoDrop Nucleic Acid Quantification*. ThermoFisher. URL: https://www.thermofisher.com/pt/en/home/industrial/spectroscopy-elemental-isotope-analysis/molecular-spectroscopy/ultraviolet-visible-visible-spectrophotometry-uv-vis-vis/uv-vis-vis-instruments/nanodrop-microvolume-spectrophotometers/nanodrop-nucleic-acid-quantification.html (visited on 10/28/2021).

[107] Pedro M Baptista et al. “The use of whole organ decellularization for the generation of a vascularized liver organoid”. In: *Hepatology* 53.2 (2011), pp. 604–617.

[108] Paul Lin et al. “Assessing porcine liver-derived biomatrix for hepatic tissue engineering”. In: *Tissue engineering* 10.7-8 (2004), pp. 1046–1053.

[109] Robert A Pouliot et al. “Porcine lung-derived extracellular matrix hydrogel properties are dependent on pepsin digestion time”. In: *Tissue Engineering Part C: Methods* 26.6 (2020), pp. 332–346.

[110] Milton T Stubbs et al. “The interaction of thrombin with fibrinogen: a structural basis for its specificity”. In: *European journal of biochemistry* 206.1 (1992), pp. 187–195.

[111] Maryam Barisam et al. “Prediction of necrotic core and hypoxic zone of multicellular spheroids in a microbioreactor with a U-shaped barrier”. In: *Micromachines* 9.3 (2018), p. 94.

[112] M.S. Attene-Ramos, C.P. Austin, and M. Xia. “High Throughput Screening”. In: *Encyclopedia of Toxicology (Third Edition)*. Ed. by Philip Wexler. Third Edition. Oxford: Academic Press, 2014, pp. 916–917. ISBN: 978-0-12-386455-0. DOI: https://doi.org/10.1016/B978-0-12-386454-3.00209-8. URL: https://www.sciencedirect.com/science/article/pii/B9780123864543002098.

[113] *ITGB1 integrin subunit beta 1 [Homo sapiens (human)]*. NCBI. URL: https://www.ncbi.nlm.nih.gov/gene/3688 (visited on 11/08/2021).

[114] *ITGB3 gene: MedlinePlus*. MedlinePlus. URL: https://medlineplus.gov/genetics/gene/itgb3/ (visited on 11/08/2021).

[115] *NOS3 gene - mutations*. GeneFood. URL: https://www.mygenefood.com/genes/heart-health-genes/nos3/ (visited on 11/08/2021).

[116] Sribalaji Lakshmikanthan et al. “Rap1 promotes VEGFR2 activation and angiogenesis by a mechanism involving integrin $\alpha v\beta 3$”. In: *Blood, The Journal of the American Society of Hematology* 118.7 (2011), pp. 2015–2026.

[117] Liping Yao et al. “The function and mechanism of COX-2 in angiogenesis of gastric cancer cells”. In: *Journal of Experimental & Clinical Cancer Research* 30.1 (2011), pp. 1–5.

[118] Bin Xiong et al. “Cyclooxygenase-2 expression and angiogenesis in colorectal cancer”. In: *World Journal of Gastroenterology: WJG* 9.6 (2003), p. 1237.

[119] Kristina Baltrunaite et al. “ETS transcription factors Etv2 and Fli1b are required for tumor angiogenesis”. In: *Angiogenesis* 20.3 (2017), pp. 307–323.

[120] Shandong Yu et al. “High concentrations of uric acid inhibit angiogenesis via regulation of the Krüppel-like factor 2-vascular endothelial growth factor-A axis by miR-92a”. In: *Circulation Journal* (2015), CJ–15.

[121] Takahiro Ueki et al. “Hepatocyte growth factor gene therapy of liver cirrhosis in rats”. In: *Nature medicine* 5.2 (1999), pp. 226–230.

[122] *HGF hepatocyte growth factor [Homo sapiens (human)]*. NCBI. URL: https://www.ncbi.nlm.nih.gov/gene?Cmd=DetailsSearch&Term=3082 (visited on 11/08/2021).

[123] Sigrid Uxa et al. “Ki-67 gene expression”. In: *Cell Death & Differentiation* (2021), pp. 1–14.

[124] *ALB albumin [Homo sapiens (human)]*. NCBI. URL: https://www.ncbi.nlm.nih.gov/gene?Cmd=DetailsSearch&Term=213 (visited on 11/08/2021).

[125] Nozlena Abdul Samad et al. “Zerumbone suppresses angiogenesis in HepG2 cells through inhibition of matrix metalloproteinase-9, vascular endothelial growth factor, and vascular endothelial growth factor receptor expressions”. In: *Pharmacognosy magazine* 13.Suppl 4 (2017), S731.

[126] M Lourdes Ponce. “Tube formation: an in vitro matrigel angiogenesis assay”. In: *Angiogenesis Protocols*. Springer, 2009, pp. 183–188.

Appendixes

APPENDIX 1 - CALIBRATION LINE FOR BCA ASSAY

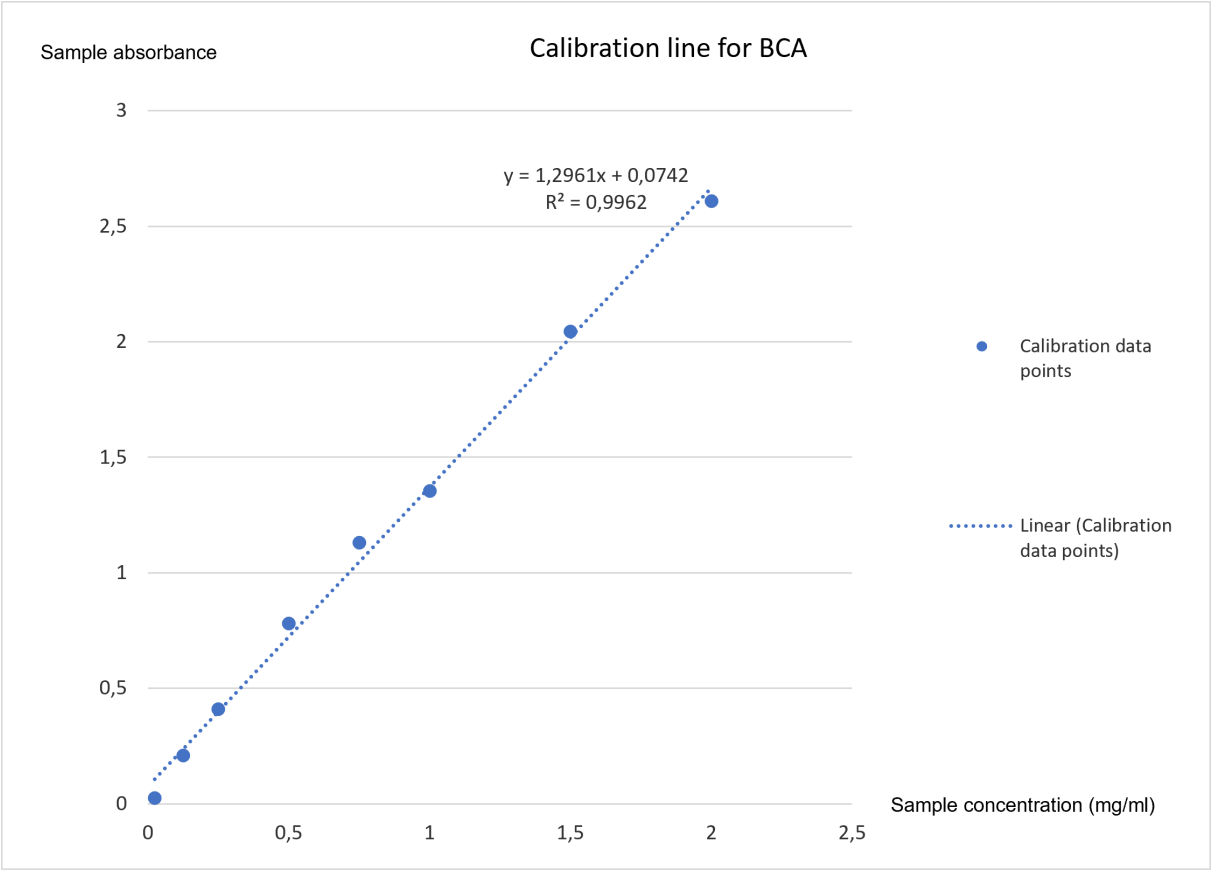

Figure 4.1: Calibration line for BCA assay based on the 562 nm absorbance of bovine serum albumine diluted in PBS